Gpr161 ciliary pools prevent hedgehog pathway hyperactivation phenotypes specifically from lack of Gli transcriptional repression

Sun-Hee Hwang[1], Bandarigoda N. Somatilaka[1,2], Kevin White[1], and Saikat Mukhopadhyay[1*].

[1]Department of Cell Biology, University of Texas Southwestern Medical Center, Dallas, Texas, 75390.

[2]Present address: Department of Dermatology, University of Texas Southwestern Medical Center, Dallas, Texas, 75390.

[*]Correspondence:

Email: Saikat.Mukhopadhyay@utsouthwestern.edu

Running title: Tissue-specific functions of ciliary Gpr161 pools.

Abstract

The primary cilium localized G-protein-coupled receptor Gpr161 represses hedgehog pathway via cAMP signaling in multiple tissues. However, whether Gpr161 functions exclusively from inside cilia is unclear. Here, we generated ciliary localization-defective but cAMP signaling-competent *Gpr161*^{mut1} knock-in mice. We uncovered distinctive roles for subcellular Gpr161 pools, contingent upon dependence of the morpho-phenotypic spectrum on downstream Gli transcriptional regulators. Compared to *Gpr161* knockout, gene dosage of the *Gpr161*^{mut1} allele caused delayed embryonic lethality, reduced upregulation of hedgehog targets and intermediate Gli3 repressor levels. Unlike *Gpr161* knockout with aberrant ventral progenitor expansion in neural tube, extraciliary Gpr161 pools in *Gpr161*^{mut1} prevented Gli2 activator-mediated ventralization. However, limb buds and midfacial tissues that require Gli repressor for morphogenesis, showed polydactyly and midface widening in *Gpr161*^{mut1} from hyperactivation. Thus, Gpr161 ciliary and extraciliary pools functioned as rheostats preventing gradations of hedgehog pathway hyperactivation. Ciliary Gpr161 pools prevented tissue-specific phenotypes dependent specifically on reduced Gli repressor thresholds.

Keywords: Cilia; hedgehog; cAMP; Gpr161; Gli repressor; neural tube; craniofacial; limb bud; polydactyly, morphogenesis.

Introduction

Hedgehog (Hh) signaling in vertebrates is an excellent system to study the role of compartmentalized cellular signaling in morphogenesis and disease (Anvarian et al. 2019; Nachury and Mick 2019). The primary cilium is a microtubule-based dynamic cellular appendage that mediates cellular signaling responses to Hh morphogens in vertebrates (Goetz and Anderson 2010; Briscoe and Therond 2013). An intricate balance between formation of Gli transcriptional activators and repressors determines the transcriptional output to Hh morphogens or in preventing precocious activation of targets (Hui and Angers 2011). Both responses are dependent on the primary cilium. Binding of Hh to its receptor Patched (Ptch1) triggers removal of Ptch1 from cilia and promotes enrichment and activation of Smoothened (Smo)—the pathway transducer—in cilia, resulting in generation of Gli transcriptional activator (GliA) (Corbit et al. 2005; Rohatgi et al. 2007). In contrast, repression in the absence of Hh involves protein kinase A (PKA)-mediated limited proteolysis of full length Gli2/3 into Gli2/3 repressor (GliR) forms, also in a cilia-dependent manner (Tuson et al. 2011; Mukhopadhyay and Rohatgi 2014). As cAMP production regulates PKA activation, studying repressive pathways regulating Hh signaling strength might provide novel insights into both spatiotemporal regulation of cAMP signaling and phenotypes arising from lack of Hh pathway repression (derepression).

We previously described that the cilia-localized orphan G-protein-coupled receptor (GPCR), Gpr161 functions as a repressor of Hh signaling during early neural tube development in mice (Mukhopadhyay et al. 2013). Mice knockout for *Gpr161* are embryonic lethal by embryonic day 10.5 (E10.5) and exhibit increased Hh signaling and expansion of ventral progenitors throughout the rostrocaudal extent of the neural tube, without disrupting cilia. Recently, *GPR161* mutations in patients suffering from caudal neural tube defects (spina bifida) have been reported (Kim et al. 2019). Gpr161 determines Gli3R formation via cAMP signaling. Interestingly, Gpr161 C-tail has been proposed to be an A-kinase anchoring protein (AKAP) for PKA activation in cilia

by binding to PKA regulatory subunit RIα and RIβ (Bachmann et al. 2016). Gpr161 is the only GPCR known to be an AKAP. In addition, the PKA regulatory subunit RIα localizes to cilia (Mick et al. 2015; Bachmann et al. 2016), whereas PKA regulatory RII subunits localize to centrosomes (Barzi et al. 2010; Tuson et al. 2011; Saade et al. 2017). Gpr161 localizes to the ciliary membrane and the recycling endocytic compartment (Mukhopadhyay et al. 2013; Pal et al. 2016). However, whether Gpr161 functions from inside the primary cilium and/or in the endomembrane compartment in regulating cAMP-PKA signaling and Hh pathway repression is not clear.

As Gpr161 is a moderately strong repressor of the Hh pathway, tissue-specific deletion of *Gpr161* has been providing us critical insights into additional developmental paradigms regulated by repression of Hh signaling through cilia. We recently described roles of Gpr161-mediated Hh pathway repression in forelimb formation, skeletal development (Hwang et al. 2018), embryonic cerebellar development (Shimada et al. 2018), and forebrain development (Shimada et al. 2019). Loss of Gpr161 and consequent Hh pathway derepression is directly relevant to the pathogenesis of pediatric cancers such as sonic hedgehog (Shh)-subtype medulloblastoma (Shimada et al. 2018; Begemann et al. 2019), skeletal dysmorphisms (Hwang et al. 2018) and forebrain abnormalities such as polymicrogyria and periventricular heterotopia (Shimada et al. 2019). Gpr161 has also be shown to a key regulator of Hh pathway repression in zebrafish in multiple tissue contexts (Tschaikner et al. 2019). However, how subcellular Gpr161 pools regulate morphogenesis of different tissues is not clear.

We recently proposed that conceptually, GliA/R regulation in different tissues can be categorized as regulation primarily by GliA or GliR thresholds, ratio sensing between GliA and GliR levels or repression by GliR in absence of Hh expression (Kopinke et al. 2020). Here, by generating a ciliary localization defective but signaling competent knock-in *Gpr161*^{mut1} mouse model, we demonstrate that tissues that mostly require Gli repressor for morphogenesis are affected specifically from loss of Gpr161 ciliary pools.

Results

A ciliary localization-defective *Gpr161* mutant is signaling-competent

We have previously described the (V/I)KARK motif in the third intracellular loop of Gpr161 to be necessary and sufficient for targeting to cilia by the tubby family protein Tulp3 (**Figure 1A**) (Mukhopadhyay et al. 2010; Mukhopadhyay et al. 2013; Badgandi et al. 2017). We used NIH 3T3 cells that are knockout for *Gpr161* (Pusapati et al. 2018) to stably overexpress untagged wildtype *Gpr161* and *Gpr161*^{mut1} (VKARK>AAAAA; Gpr161^{mut1}). Wildtype Gpr161 predominantly localized to cilia. In contrast, Gpr161^{mut1} was not localized to cilia but was observed in vesicles surrounding the base of cilia (**Figure 1B**). We had previously demonstrated such periciliary Gpr161 containing vesicles to be recycling endosomes that co-label with the endocytosed transferrin (Mukhopadhyay et al. 2013).

INPP5E knockdown increases levels of TULP3, IFT-A and TULP3 cargoes in the ciliary membrane (Garcia-Gonzalo et al. 2011; Chavez et al. 2015). If Gpr161^{mut1} transits through cilia but is too low to detect at steady state, we would expect to see it accumulating upon *INPP5E* knockdown. By stably expressing the mutant LAP-tagged wild type (*Gpr161*^{wt}) and *Gpr161*^{mut1} in RPE hTERT cells, we confirmed the *Gpr161*^{mut1} fusion to be not localizing to cilia unlike *Gpr161*^{wt} (LAP, S tag-PreScission-GFP) (**Figure 1C-D**). Upon *INPP5E* knockdown, we saw accumulation of endogenous TULP3 in cilia (**Figure 1C-D**). However, upon *INPP5E* knockdown in LAP-tagged *Gpr161*^{Mut1} expressing cells, we did not see any accumulation of the mutant receptor in cilia (**Figure 1C-D**), despite accumulation of TULP3, suggesting that this mutant form does not transit through cilia.

Agonist-independent constitutive signaling has now been observed for a wide variety of GPCRs (Leurs et al. 1998; Seifert and Wenzel-Seifert 2002). In the absence of a known ligand, we previously demonstrated constitutive activity of the orphan Gpr161 by generating doxycycline-inducible stable cell lines expressing the untagged wild-type receptor (Mukhopadhyay et al. 2013).

We used a similar strategy to generate a doxycycline-inducible line expressing untagged *Gpr161*^{mut1}. We used a TR-FRET cAMP assay (Cisbio) for estimating cAMP levels. These assays eliminate the background noise due to FRET-based estimation of signals, and the use of long-lived fluorophores (in this case lathanides), combined with time-resolved FRET detection (a delay between excitation and emission detection) minimizes prompt intrinsic fluorescence interferences (Degorce et al. 2009). Gpr161^{mut1} demonstrated comparable constitutive cAMP signaling activity compared to the wild-type receptor (**Figure 1E**), suggesting that the ciliary localization defective GPCR was signaling competent. Thus, the *Gpr161*^{mut1} mutant allows in uncoupling cAMP signaling function from ciliary localization of Gpr161.

Generating ciliary localization defective endogenous knock-in *Gpr161*^{mut1} mouse model

We next generated a mouse knock-in allele of *Gpr161*^{mut1} in the endogenous locus and confirmed the endogenous integration by southern blotting (**Figure 2A-B**) and sequencing (**Figure 2C**). We engineered a NotI restriction site in the mutated *Gpr161*^{mut1} exon 4 sequence (**Figure 2-figure supplement 1**) for genotyping using RFLP assays (**Figure 2A, 2D**). We bred the knock-in alleles with *Gpr161* knockout (ko) allele. Quantitative RT-PCR of *Gpr161* transcripts in E9.5 embryos suggested that the *Gpr16*^{mut1} transcript was expressed at similar levels compared to wild type and was reduced to 50% compared to wildtype in *Gpr161*$^{ko/mut1}$ embryos (**Figure 2E**). *Gpr161*$^{ko/ko}$ embryos lacked *Gpr161* transcripts, as expected. We were unable to determine protein stability of the mutant receptor in the *Gpr161*^{mut1} embryos due to technical constraints in immunoblotting for endogenous levels**.** However, we note Gpr161^{mut1} in vesicles surrounding the base of cilia (**Figure 1B**) and constitutive cAMP signaling activity (**Figure 1G**) in overexpressed stable cell lines, suggesting that protein levels and activity of the mutant were comparable with wild type Gpr161.

***Gpr161*^{mut1} allele is hypomorphic to knockout**

Mice homozygous for *Gpr161* ko allele are embryonic lethal by E10.5 with extensive craniofacial

abnormalities, open forebrain and midbrain regions, and lack of forelimbs (Mukhopadhyay et al. 2013; Hwang et al. 2018) (**Figure 3A**). In contrast, the *Gpr161*$^{mut1/ko}$ mice were embryonic lethal by E13.5 (**Table 1**). The *Gpr161*$^{mut1/ko}$ embryos had craniofacial abnormalities, microphthalmia (**Figure 3A-C**) and spina bifida similar to *Gpr161* ko (**Figure 3B**) along with kinked tail, often associated with caudal neural tube defects (**Figure 3C**). They also had stunted forelimbs (**Figure 3B-C**) and heart defects with pericardial effusion (**Figure 3C**). However, the *Gpr161*$^{mut1/mut1}$ mice were embryonic lethal by E14.5 (**Table 1**) with craniofacial abnormalities including mid face widening, microphthalmia (**Figure 3D-E**) and polydactyly in both forelimbs and hindlimbs (**Figure 3D**). Thus, the *Gpr161*^{mut1} allele is hypomorphic to *Gpr161* ko. The *Gpr161*$^{mut1/mut1}$, *Gpr161*$^{mut1/ko}$ and *Gpr161*$^{ko/ko}$ embryos give rise to an allelic series with earlier embryonic lethality and increasing phenotypic severity.

Gpr161$^{mut1/ko}$ embryos have reduced Hh pathway hyperactivation compared to knockouts

As *Gpr161*^{mut1} allele is later embryonic lethal compared to knockout, we tested if Hh signaling is impacted in *Gpr161* mutants by analyzing the expression of direct transcriptional targets of the Hh pathway, *Gli1* and *Patched2* (*Ptch2*). In whole embryo extracts at E9.5, we detected increased levels of both transcripts in the *Gpr161*$^{ko/ko}$ embryos, intermediate levels in *Gpr161*$^{mut1/ko}$ embryos, and slightly elevated levels but statistically insignificant from wild type in *Gpr161*$^{mut1/mut1}$ embryos (**Figure 4A-B**). Gli1 protein levels also showed similar trends (**Figure 4C**). In summary, these data indicate that *Gpr161* knock-in mutants experience gradually decreasing levels of Hh pathway hyperactivity compared to ko, commensurate with monoallelic or biallelic expression of *Gpr161*^{mut1}.

Gpr161$^{mut1/ko}$ embryos have intermediate GliR levels compared to knockouts

In the absence of Hh ligand, PKA-mediated phosphorylation of Gli3 results in its limited proteolysis into Gli3R (Wang et al. 2000; Tempe et al. 2006; Niewiadomski et al. 2014). In *Gpr161*$^{ko/ko}$ embryos, the extent of Gli3 processing into Gli3R at E9.5 whole-embryonic extracts was strongly

decreased compared to wild type, suggesting that Gpr161 directs processing of Gli3 into Gli3R (Mukhopadhyay et al. 2013; Hwang et al. 2018). Compared to wild-type, the extent of Gli3 processing into Gli3R at E9.5 whole-embryonic extracts was strongly decreased in *Gpr161*$^{ko/ko}$ and *Gpr161*$^{ko/mut1}$ embryos, and trended towards decreased levels, but were not statistically significant in the *Gpr161*$^{mut1/mut1}$ embryos. Upon Hh signaling limited proteolysis of Gli3 is prevented, whereas activated full-length Gli proteins are formed that are unstable (Chen et al. 2009; Jia et al. 2009; Humke et al. 2010; Wang et al. 2010; Wen et al. 2010). Compared to wild type, Gli3 full-length forms trended towards decrease in *Gpr161*$^{ko/mut1}$ and *Gpr161*$^{mut1/mut1}$ embryos but were not statistically significant (**Figure 4C**). Gli3 full-length to Gli3R ratios were significantly increased in both *Gpr161*$^{ko/ko}$ and *Gpr161*$^{ko/mut1}$ embryos with respect to wild type (**Figure 4C**). Gli2R levels were only moderately reduced in *Gpr161*$^{ko/ko}$ embryos at E9.5, while being less affected in the *Gpr161*$^{ko/mut1}$ and *Gpr161*$^{mut1/mut1}$ embryos (**Figure 4-figure supplement 1**). In summary, the *Gpr161* mutants exhibit gradually decreasing severity of Gli3 processing defects compared to ko, commensurate with monoallelic or biallelic expression of *Gpr161*^{mut1}.

Gpr161^{mut1} NIH 3T3 cells exhibit Gli2 accumulation in cilia similar to *Gpr161* knockouts

Upon Hh pathway activation, Gli2 proteins accumulate at the tips of cilia (Haycraft et al. 2005; Chen et al. 2009; Kim et al. 2009). While ~20% of cilia tips in control cells had detectable Gli2 staining, treatment with SAG increased Gli2 accumulation in control cilia in NIH 3T3 cells (**Figure 4D-E**). In contrast, ~60% of *Gpr161* ko cilia in NIH 3T3 cells had Gli2 staining irrespective of SAG treatment (**Figure 4D-E**). Stable expression of wild type *Gpr161* (*Gpr161*^{wt}), but not that of *Gpr161*^{mut1}, rescued the basal Gli2 ciliary accumulation in *Gpr161* ko cells. Thus, basal Gli2 accumulation in ciliary tips occurs from the absence of ciliary Gpr161 pools.

Gpr161$^{mut1/ko}$ embryos exhibit less ventralized neural tube compared to *Gpr161* knockouts

The neural tube is patterned during early embryonic development by Hh secreted from the notochord. The neuroprogenitors acquire different spatial identities along the dorso-ventral axis

due to a complex interplay of transcription factors, which are expressed in response to relative variations in Hh levels, as well as the duration for which they are exposed (Dessaud et al. 2008). As we had demonstrated before (Mukhopadhyay et al. 2013), Hh-dependent ventral cell types were ectopically specified at the expense of lateral and dorsal cell types (ventralization) in the *Gpr161*$^{ko/ko}$ at E9.5 (**Figure 5**). Specifically, floor plate progenitors expressing FoxA2, and p3/pMN/p2 progenitors expressing Nkx6.1 showed enlarged expression domains, expanding into comparatively more dorsal regions throughout the rostrocaudal extent of the spinal cord and hindbrain (**Figure 5**). The dorsolateral neural tube marker Pax6 was expressed in dorsally restricted domains, whereas Pax7 was strongly downregulated (**Figure 5**).

Ventralmost neural tube patterning is dependent on the downstream activation of Gli2 (Bai and Joyner 2001), whereas intermediate-level patterning is Gli3R regulated (Persson et al. 2002). We investigated if the *Gpr161* ko phenotype is dependent on Gli2 by generating *Gpr161; Gli2* double ko. We generated linked double mutants by recombination, as *Gpr161* and *Gli2* genes are on the same chromosome. *Gli2* single ko is perinatal lethal (Bai and Joyner 2001). The *Gpr161; Gli2* double ko survived till E12.75, past the embryonic lethality period for *Gpr161* single ko at E10.5. The double ko embryos also exhibited exencephaly, similar to *Gpr161* ko (**Figure 5**), suggesting a possible role for Gli3 in this region (Yu et al. 2009; Liu et al. 2015; Shimada et al. 2019).*Gli2* ko shows sparse FoxA2 expression in the floorplate throughout the rostrocaudal extent of the neural tube without affecting Nkx6.1, compared to wild type (Somatilaka et al. 2020). The double ko had reduced FoxA2 in floor plate compared to *Gpr161* ko, suggesting that ventralization requires Gli2A. However, persistent but limited ventralization of Nkx6.1 domain suggested independence from Gli2A (**Figure 5**). The dorsolateral markers Pax7 and Pax6 were both partially restored compared to *Gpr161* ko (**Figure 5**). Thus, ventralization of FoxA2 in *Gpr161* ko is Gli2-dependent, whereas Nkx6.1 domain ventralization is likely to be Gli3R-dependent.

As we had detected a partial hyperactivation of Hh targets and decrease in Gli3R levels in *Gpr161*$^{ko/mut1}$ whole embryo lysates (**Figure 4**), we next compared the neural tube phenotypes

of *Gpr161*$^{ko/mut1}$ and *Gpr161*$^{mut1/mut1}$ embryos with *Gpr161*$^{ko/ko}$ and *Gpr161; Gli2* double ko. In contrast to *Gpr161*$^{ko/ko}$, *Gpr161*$^{ko/mut1}$ embryos had normal FoxA2 expression limited to floor plate. However, Nkx6.1 was expanded dorsally, although lesser in extent than in *Gpr161*$^{ko/ko}$. Pax6 was not dorsally restricted, whereas Pax7 was restored, unlike *Gpr161*$^{ko/ko}$ (**Figure 5**). Neural tube patterning in *Gpr161*$^{mut1/mut1}$ embryos was almost similar to wild type, except for a more restricted mid-dorsal expression of Pax7 (**Figure 5**). Thus, ventral most FoxA2 patterning was unaffected in *Gpr161*$^{ko/mut1}$ and *Gpr161*$^{mut1/mut1}$ embryos, unlike *Gpr161* ko, suggesting that ventral most progenitor expansion that requires Gli2A does not occur upon loss of ciliary Gpr161 pools. The persistence of limited Nkx6.1 ventralization in *Gpr161*$^{ko/mut1}$ and *Gpr161; Gli2* double ko phenocopies lack of Gli3 repressor (Persson et al. 2002). Thus, ciliary pools of Gpr161 are required for generating sufficient Gli3R levels to prevent such intermediate level ventralization. Increased extracellular Gpr161 pools in *Gpr161*$^{mut1/mut1}$ also prevent Nkx6.1 ventralization from likely restoration of Gli3R.

Gpr16$^{mut/mut11}$ embryos exhibit high Hh signaling and polydactyly in limb buds

As neural tube patterning defects were minimal in *Gpr161*$^{mut1/mut1}$ embryos, we tested if other tissues affected by Hh signaling were affected. *Shh* is expressed from the zone of polarizing activity (ZPA) in posterior limb buds starting around E9.75 in the fore limbs (Charite et al. 2000) and patterns the digits (Niswander 2003). Mutual antagonism between Gli3R and the bHLH transcription factor, dHand prepatterns the forelimb mesenchyme before *Shh* expression in causing posterior expression of *bona fide* Shh pathway targets and of 5' *Hoxd* genes such as *Hoxd13* (te Welscher et al. 2002). dHand also drives Shh expression from ZPA (Charite et al. 2000). *Gpr161*$^{ko/ko}$ embryos lack forelimbs and have increased Shh signaling in the hind limbs (Hwang et al. 2018). Depletion of *Gpr161* in the limb mesenchyme using *Prx1-Cre* (*Prx1-Cre; Gpr161*$^{f/f}$) results increased expression of *Ptch1/Gli1* in both anterior and posterior forelimb fields and ectopic expression of Shh anteriorly. In contrast to *Gpr161*$^{ko/ko}$, forelimb buds were formed in

Gpr161$^{mut1/mut1}$ embryos, and as in *Prx-Cre; Gpr161*$^{f/f}$ there was increased expression of *Ptch1/Gli1* in both anterior and posterior forelimb and hindlimb fields, as detected by RNA in-situ hybridization (RNA ISH) (**Figure 6A**).

Several features suggested a lack of Gli3R antagonism in causing Shh pathway hyperactivation. First, Shh was diffusely expressed posteriorly at E10.5 as detected by RNA ISH (**Figure 6B**), a likely result of dHand misexpression from Gli3R lack. Ectopic anterior expression of Shh in *Prx1-Cre; Gpr161*$^{f/f}$ is also likely from Gli3R lack that manifests later in the limb mesenchyme (Hwang et al. 2018). Second, *Hoxd13* expression by RNA ISH was anteriorly expanded in *Gpr161*$^{mut1/mut}$ embryos at E10.5 (**Figure 6C**), a likely result of lack of Gli3R-antagonism (te Welscher et al. 2002). Third, we noticed a reduction of Gli3R formation in limb buds of *Gpr161*$^{mut1/mut1}$ embryos by immunoblotting at E12.5 (**Figure 6D**).

By E13.5, *Prx1-Cre; Gpr161*$^{f/f}$ had increased number of digit fields resulting in polysyndactylous phenotypes (Hwang et al. 2018) (**Figure 6E**). *Gpr161*$^{mut1/mut1}$ embryos also showed polydactyly in both forelimb and hindlimb buds as apparent from RNA ISH for *Sox9* and *Col2a1* for mesenchymal and chondrogenic condensations, respectively (**Figure 6E**). Thus, lack of Gli3R in *Gpr161*$^{mut1/mut1}$ embryos is sufficient to cause increased Shh signaling and polydactyly.

Gpr161$^{mut1/mut1}$ embryos show high Hh signaling and mid face widening

Similar to limb bud patterning we tested if other tissues affected by lack of Gli repressor are similarly affected from loss of ciliary pools of Gpr161. Loss of cilia in cranial neural crest cells causes midfacial widening, duplicated nasal septum and bilateral cleft secondary palate (Brugmann et al. 2010; Chang et al. 2016). Deletion of both *Gli2* and *Gli3* phenocopies these phenotypes, which are restored by expression of Gli3R (Chang et al. 2016), suggesting that ciliary signaling regulate GliR formation that is important in morphogenesis of this tissue. While lack of cilia in *Wnt1-Cre; Kif3a*$^{f/f}$ mutants shows lack of Gli2/3 repressor levels, expression of *Ptch1* and *Gli1* are asynchronized, and are not reflective of the derepression (Chang et al. 2016).

Cranial neural crest-specific deletion of *Gpr161* using *Wnt1-Cre* resulted in microphthalmia, severe midfacial cleft and widening (**Figure 7A, D**). Similar midfacial widening as evident from increased distance between nasal pits was also observed in the *Gpr161*$^{mut1/mut1}$ embryos (**Figure 7B-E**). The midfacial widening resulted from increased gap between maxillary processes by ingression of median nasal processes (**Figure 7B-C**). *Gpr161*$^{mut1/mut1}$ embryos had high Hh signaling in craniofacial structures including nasopharangeal processes, palatal shelves and tongue, as evident from high *Ptch1* transcript levels by RNA ISH (**Figure 7B**). We also noted increased *Gli1* levels in the tongue of *Gpr161*$^{mut1/mut1}$ embryos by RNA ISH (**Figure 7C**). *Gpr161; Gli2* double ko embryos also showed midfacial widening and high *Ptch1* transcript levels by RNA ISH in the nasopharangeal processes (**Figure 7F**). Thus, high Hh signaling and midfacial widening from loss of Gpr161 ciliary pools was not Gli2A-dependent but was likely from lack of GliR.

Discussion

Gpr161^{mut1} establishes an allelic series in regulating Hh pathway derepression

Our results establish that Gpr161 ciliary pools, by generating sufficient Gli repressor, prevents moderate level Hh pathway hyperactivation, whereas both ciliary and extraciliary pools need to be absent for highest levels of pathway hyperactivity. The continuum of Hh pathway transcriptional upregulation and Gli3R processing defects between *Gpr161* ko, *Gpr161*$^{mut1/ko}$ and *Gpr161*$^{mut1/mut1}$ establishes an allelic series for *Gpr161*, showing that Gpr161 ciliary and extraciliary pools function as a rheostat in regulating Hh signaling strength. The distinct phenotypic consequences in different tissues, however, argues for a more discontinuous and thresholded response to GliA/R levels. Tissue regions that depend on Gli repressor thresholds are specifically affected from loss of ciliary pools of Gpr161. These regions include the developing limb buds, face and intermediate regions of the neural tube. Therefore, the effects of ciliary loss of Gpr161 pools are tissue-specific and dependent on the particular requirements of the specific tissues on GliR vs GliA in the morpho-phenotypic spectrum.

Gpr161 ciliary and extraciliary pools cumulatively contribute to Gli-repressor formation

Gpr161 pools both inside and outside cilia cumulatively contribute to Gli3R processing, with increased outside pools in *Gpr161*$^{mut1/mut1}$ embryos increasing processing levels compared to *Gpr161*$^{mut1/ko}$ embryos. However, *Gpr161*$^{mut1/mut1}$ limb buds showed decreased Gli3R processing compared to whole embryo lysates, suggesting limited compensation by extracellular Gpr161 pools in the limb buds. Gpr161 activity outside cilia is probably through the periciliary recycling endosomal compartment where it localizes in addition to cilia (Mukhopadhyay et al. 2013). Gpr161-regulated cAMP production in the endomembrane compartment, as reported for other GPCRs (Calebiro et al. 2009; Kotowski et al. 2011; Irannejad et al. 2013; Vilardaga et al. 2014; Crilly and Puthenveedu 2020), could be relevant for cumulative contributions to GliR processing. Direct Gpr161 C-tail binding to PKA RIα and RIβ regulatory subunits (Bachmann et al. 2016)

could also facilitate PKA activation in close proximity to Gpr161-mediated cAMP production for GliR processing.

Gpr161 ciliary and extraciliary pools uncouple Gli2 accumulation in ciliary tips from activator formation

As GliA and GliR are generated from the same parental template, GliA formation is inherently dependent on GliR processing (Pan et al. 2006). C-term phosphorylation causes GliR formation, whereas GliA formation is dependent on lack of C-term phosphorylation (Niewiadomski et al. 2014). *Gpr161* ko cells show Gli2 accumulation in cilia irrespective of pathway activation, and such accumulation persists upon *Gpr161*^{mut1} expression in ko cells. Similar basal accumulation of Gli2 in cilia has also been observed in resting *PKA* null MEFs (Tuson et al. 2011) and cells lacking Ankmy2, an ankyrin repeat and MYND domain protein that regulates adenylyl cyclase trafficking to cilia (Somatilaka et al. 2020). Gli2A formation is, however, compromised in *Gpr161*$^{mut1/mut1}$ embryos in the neural tube. While Gli2R formation is much less efficient than Gli3R formation, lack of Gpr161 both inside and outside cilia is required for fully dephosphorylated Gli2, which has been shown to function as an activator in neural tube ventralization (Niewiadomski et al. 2014). Gli2 accumulation in cilia in the absence of ciliary Gpr161 pools suggest such accumulation to be upstream of full scale Gli2 activation and probably arises from restricted Gli2 phosphorylation insufficient to cause discernible processing defects.

Gpr161 ciliary pools regulate Hh repression-regulated morpho-phenotypic spectrum

Although Gli family members bind to same consensus DNA sequences, GliA and GliR levels are differentially involved in sculpting tissues, likely from context-dependent cis-regulation of targets by co-activators/repressors (Oosterveen et al. 2012). Alternatively, tissue-specific regulation of enhancer activity regulates Gli-mediated repression (Lex et al. 2020). We recently conceptually simplified the complexity in Hh regulation in tissues based on genetic epistasis of Hh mutants with *Gli2* ko and *Gli3R* alleles. Phenotypes rescued by Gli3R are GliR-dependent, whereas those

rescued by Gli2 loss are likely to be Gli2A-dependent. Hh-dependent morphogenesis can be categorized in different tissues as regulation primarily by GliA or GliR thresholds, ratio sensing between GliA and GliR levels or repression by GliR in absence of Hh expression (Falkenstein and Vokes 2014; Kopinke et al. 2020). Morphogenesis in tissues that are patterned by Hh and predominantly require Gli2 and Gli3 activation, such as the ventral neural tube, show lack of activation phenotypes with loss of cilia. In contrast, tissues that require Gli repressor thresholds, such as midface and limbbuds, show lack of repression phenotypes with loss of cilia (Goetz and Anderson 2010).

Ventral part of the neural tube is mainly regulated by Gli2 and Gli3 activators (Bai and Joyner 2001; Bai et al. 2004), whereas intermediate levels of neural tube are regulated by Gli3 repressor levels (Persson et al. 2002). Complete lack of *Gpr161* causes expansion of the ventral, including ventral most progenitors rostrocaudally (Mukhopadhyay et al. 2013). However, lack of Gpr161 ciliary pools in *Gpr161*$^{mut1/ko}$ prevent ventral most progenitor expansion but retains ventral expansion of Nkx6.1 in the intermediate levels of neural tube. Thus, lack of ciliary Gpr161 pools prevent sufficient Gli3R processing required to inhibit intermediate level ventralization (**Figure 8A**). Furthermore, restoration of Gli3R by increased extracellular Gpr161 pools in *Gpr161*$^{mut1/mut1}$ prevents such intermediate level ventralization of Nkx6.1. Lack of the cilia localized atypical GTPase, Arl13b, results in both ventral and dorsal expansion of intermediate Shh-dependent cell fates (Caspary et al. 2007). However, such regulation does not require ciliary pools of Arl13b, suggesting Arl13b functions outside cilia in these contexts (Gigante et al. 2020). *Gpr161*$^{mut1/ko}$ embryos also show exencephaly and spina bifida, similar to *Gpr161* ko (Mukhopadhyay et al. 2013). While mutants causing Hh pathway hyperactivation are associated with neural tube defects (Ybot-Gonzalez et al. 2002; Murdoch and Copp 2010; Somatilaka et al. 2020), cross-regulation with other pathways including Wnt (Zhao et al. 2014) and BMP signaling (Ybot-Gonzalez et al. 2007) could determine neural tube closure at different spinal levels. Role of ciliary Gpr161 pools in regulation of these pathways with relation to neural tube closure is presently unclear. A ciliary

retained but PKA-RI non-binding *Gpr161*^{vl} truncation mutant (Bachmann et al. 2016; Pal et al. 2016) is also associated with spina bifida (Matteson et al. 2008), and could involve Wnt signaling defects (Li et al. 2015).

Lack of Gpr161 ciliary pools in both limb buds shows increased Hh pathway targets and expanded *Hoxd13* from lack of Gli3R contributing to polydactyly. We do not see ectopic Shh expression as in *Prx1-Cre; Gpr161*$^{f/f}$ (Hwang et al. 2018); instead, the Shh expression in the posterior limb bud is diffuse, probably from deficient counter-antagonism between Gli3R and dHand (Charite et al. 2000; te Welscher et al. 2002), which drives Shh expression (Charite et al. 2000). Similarly, a hypomorphic *Ift88* mutant that causes short cilia causes premature expansion of *dHand* before Shh expression suggesting compromised Gli3R formation and preaxial polydactyly without ectopic Shh expression (Liu et al. 2005). Forelimb buds are also completely lacking in *Gpr161*$^{ko/ko}$ embryos (Hwang et al. 2018), presumably from high Hh signaling in the presumptive limb fields. Therefore, the lack of Gpr161 pools in cilia demonstrate effects from moderate levels of derepression of Hh pathway (**Figure 8B**).

Shh is expressed from the frontonasal ectodermal zone (FEZ) in the medial nasal processes (Hu and Marcucio 2009). Midfacial tissues are regulated by Gli2R and Gli3R levels in normal morphogenesis in preventing midfacial widening (Chang et al. 2016; Schock and Brugmann 2017). Lack of Gpr161 ciliary pools phenocopies *Gpr161* deletion in cranial neural crest using *Wnt1-Cre* in showing midfacial widening similar to loss of cilia or lack of Gli2 and Gli3 (Brugmann et al. 2010; Chang et al. 2016). The facial phenotypes are accompanied by increased levels of *Ptch1* and *Gli1* transcripts in the mid-facial tissues. However, conventional pathway outputs such as *Ptch1* and *Gli1* expression are not increased in the affected tissues upon ciliary loss (Chang et al. 2016), suggesting Hh hyperactivation to be stronger upon *Gpr161* loss from cilia. Cilia regulates both GliA and GliR; therefore, loss of cilia, despite causing lack of repression, might not be as effective in causing pathway hyperactivation as *Gpr161* loss. The craniofacial phenotypes and upregulation of *Ptch1* transcripts persists in mid face of *Gpr161; Gli2* double ko,

consistent with derepression from lack of GliR in causing the mid-facial phenotypes (**Figure 8C**).

By establishing the allelic series for Gpr161-mediated Hh pathway repression, we are also poised to unravel neomorphic phenotypic outcomes from varying signaling strength of Hh signaling. We note defects in the heart in the *Gpr161*$^{mut1/ko}$ embryos, which include ventricular hypoplasia and pericardial effusion, but less so, at least grossly, in the *Gpr161*$^{mut1/mut1}$ embryos. Future studies will determine the role of Hh pathway repression in cardiogenesis (Constable and Mukhopadhyay 2020) and in morphogenesis of other tissues.

Material and Methods

EXPERIMENTAL MODEL AND SUBJECT DETAILS

ES cells

A BAC overlapping the mouse *Gpr161* genomic locus was engineered by recombineering using an FRT-PGKneo-FRT selection cassette. The required mutation (with an engineered NotI site) was separated from the selection cassette by 536 bp (Lee et al. 2001). Recombineering was done by the Biomedical Research Core Facility, University of Michigan (Zeidler et al. 2011). The exon 4 fragments of the *Gpr161^{mut1}* targeting construct was generated using this engineered BAC (#RP23-235-E18) by further cloning into a modified pGKneoloxP2.DTA.2 vector as follows. The pGKneoloxP2.DTA.2 vector was digested with SacII and NheI and religated. The left arm consisting of 4100 bp upstream and the right arm consisting of 4800 bp downstream of the FRT-PGKneo-FRT cassette in the BAC were PCR cloned into the HindIII site of this modified vector (**Figure 2, figure supplement 1**). The engineered plasmid was linearized with XhoI and was electroporated into JM8.N4 ES cells at the Transgenic Core in UT Southwestern, Dallas (Figure 2C). From among 469 ES cell clones, 56 clones were first screened by PCR, and two clones 4D9 and 5F9 were further screened by southern blotting with probes as marked in Figure 2A. ES cells were grown on SNL feeders with media containing 20% Serum, 6 mM L-glutamine, 1X Penicillin/Streptomycin, 1 mM β-mercaptoethanol, 1 mM Non-essential Amino Acids, 1X Nucleosides, 10 mg/L Sodium Pyruvate, ESGRO supplement 66 μl/L and incubated at 37 ^{0}C in 5% CO_2 (Dr. Robert Hammer lab, UT Southwestern, Dallas).

Mouse strains

The *Gpr161$^{mut1\text{-}neo/+}$* ES cells (5F9 clone) were injected into host embryos of the C57BL/6 albino strain by the transgenic core (Dr. Robert Hammer lab, UT Southwestern Medical Center, Dallas). Mice with germline transmission were crossed with Flp-O (Jackson lab; Stock no: 012930) for deleting the FRT-PGKneo-FRT cassette to generate the *Gpr161^{mut1}* allele. The *Gpr161* knockout and conditional allele targeting the third exon crossed has been described before (Hwang et al. 2018). Double knockout analysis was performed using *Gli2^{tm1Alj}* (ko) allele (Mo et al. 1997). *Prx1-Cre* ((Logan et al. 2002); Jax strain No: 005584) or *Wnt1-Cre* ((Lewis et al. 2013); Jax strain No: 022501) was crossed with the *Gpr161$^{f/f}$*. The *Gli2 ko* and *Gpr161* floxed alleles were linked through genetic recombination by breeding *Gpr161$^{f/f}$* with *Gli2$^{ko/+}$* animals. Crossing with CAG-Cre recombinase line (Sakai and Miyazaki 1997), in which Cre is expressed ubiquitously, generated the linked *Gpr161; Gli2* double knockout allele. Yolk sac DNA was used for genotyping embryos. Mice were housed in standard cages that contained three to five mice per cage, with water and standard diet *ad libitum* and a 12 h light/dark cycle. Noon of the day on which a vaginal plug was found was considered E0.5. All the animals in the study were handled according to protocols approved by the UT Southwestern Institutional Animal Care and Use Committee, and the mouse colonies were maintained in a barrier facility at UT Southwestern, in agreement with the State of Texas legal and ethical standards of animal care.

Stable cell lines

The *Gpr161* ko NIH 3T3 Flp-In cell line was a gift from Rajat Rohatgi (Pusapati et al. 2018). The cells were cultured in DMEM-high glucose media (D5796; Sigma) with 10% BCS (Sigma-Aldrich), 0.05 mg/ml penicillin, 0.05 mg/ml streptomycin, and 4.5 mM glutamine. Stable knockout cell lines were generated by retroviral infection with pBABE constructs having untagged wild type or mutant *Gpr161* inserts followed by antibiotic selection. RPE hTERT cells were grown in DMEM F12 media with 10% FBS (Sigma-Aldrich), 0.05 mg/ml penicillin, 0.05 mg/ml streptomycin, and 4.5 mM glutamine. RPE hTert cells were retrovirally infected with C-term LAP-tagged *Gpr161* wild type or mutant constructs and flow sorted for GFP after puromycin selection. Stable doxycycline-inducible

NIH 3T3 Tet-on 3G cells expressing untagged *Gpr161* and *Gpr161^{mut1}* receptor variants were generated by retroviral infection. These cell lines were grown in Tet-free serum (Clontech) until induction by Doxycycline (Mukhopadhyay et al. 2013). Single, multiple amino acid mutations, or deletions in full-length Gpr161 were generated using Quikchange site-directed mutagenesis kit (Stratagene or Q5 Mutagenesis Kit (NEB).

METHOD DETAILS

Mouse genotyping

Genotyping of *Gpr161 mut1* alleles were performed using primers in the intron 3-4 (5' CAGAAAGCAACAGCAAAGCA) and intron 4-5 (5' ACCCTGACACTGCCCTTAGC). The PCR product of wild type and *mut1* allele bands were 917 and 950 bp, respectively. Only the PCR product from the *mut1* allele was digested into 420 and 530 bp products with NotI. Genotyping of *Gpr161* knockout or floxed alleles were performed using primers in the deleted 4th exon (5' CAAGATGGATTCGCAGTAGCTTGG), flanking the 3' end of the deleted exon (5' ATGGGGTACACCATTGGATACAGG), and in the Neo cassette (5' CAACGGGTTCTTCTGTTAGTCC). Wild type, floxed and knockout bands were 816, 965, and 485 bp, respectively (Hwang et al. 2018). *Cre* allele was genotyped with Cre-F (5'-AAT GCT GTC ACT TGG TCG TGG C-3') and Cre-R (5'-GAA AAT GCT TCT GTC CGT TTG C-3') primers (100 bp amplicon). Wild type and knockout bands were 340 bp and 490 bp, respectively. To genotype *Gli2* mice, Gli2 sense (5'-AAA CAA AGC TCC TGT ACA CG-3'), Gli2 antisense (5'-CAC CCC AAA GCA TGT GTT TT-3') and pPNT (5'-ATG CCT GCT CTT TAC TGA AG-3') primers were used. Wild type and knockout bands were 300 bp and 600 bp, respectively.

siRNA transfection

RPE hTERT cells were passaged on glass coverslips and transfected with siRNA using Lipofectamine RNAiMax (Invitrogen). 100 nM siRNA was transfected during plating followed by 100 nM reverse transfection 24h after plating. The OTP siRNA sequences are as follows: INPP5E (J-020852-05) 5′-GGAAUUAAAAGACGGAUUU-3′ (Humbert et al., 2012). OTP nontargeting pool (GE Healthcare) was used as control siRNAs in all experiments. 72h after first transfection, the cells were starved with 0.2 % FBS starving media for 24h and fixed in 4% paraformaldehyde (PFA) for immunofluorescence.

TR-FRET cAMP assays

We used a TR-FRET cAMP assay (Cisbio) for estimating cAMP as these assays eliminate the background noise due to FRET-based estimation of signals. Also, the use of long-lived fluorophores (in this case lathanides), combined with time-resolved detection (a delay between excitation and emission detection) minimizes prompt intrinsic fluorescence interferences (Degorce et al. 2009). TR-FRET assays on stable doxycycline-inducible NIH 3T3 Tet-on 3G cells expressing *Gpr161* or *Gpr161^{mut1}* were performed according to manufacturer's instructions (Cisbio) (Mukhopadhyay et al. 2013). Cells were plated on 96 well poly-D-lysine coated plates and induced with doxycycline (2 ug/ml) for 24 hrs. Cells were finally treated with the nonselective phosphodiesterase inhibitor IBMX (1mM). Individual treatments were run in each experiment in triplicate. The final FRET counts were recorded using an EnVision 2103 multiplate reader (Perkin Elmer). Standard curves were generated using least squares fitting method (with R^2 value >0.99) and values for unknowns were interpolated using Graphpad Prism.

Tissue processing, antibodies, immunostaining and microscopy

Mouse embryos fixed in 4% PFA overnight at 4°C and processed for cryosectioning. For cryosectioning, the embryos were incubated in 30% sucrose at 4°C until they were submerged in the solution. Embryos were mounted with OCT compound. Embryos in OCT were cut into 15 µm

frozen sections. The sections were incubated in PBS for 15 min to dissolve away the OCT. Sections were then blocked in blocking buffer (1% normal donkey serum [Jackson immunoResearch, West Grove, PA] in PBS) for 1 h at room temperature. Sections were incubated with primary antibodies against the following antigens; overnight at 4°C: FoxA2 (1:1000, ab108422; Abcam), Nkx6.1 (1:100, F55A10-s; DSHB), Pax6 (1:2000, 901301; Biolegend), Pax7 (1:10; DSHB). After three PBS washes, the sections were incubated in secondary antibodies (Alexa Fluor 488-, 555-, 594-, 647- conjugated secondary antibodies, 1:500; Life Technologies, Carlsbad, CA or Jackson ImmunoResearch) for 1 h at room temperature. Cell nuclei were stained with DAPI (Sigma). Slides were mounted with Fluoromount-G (0100-01; Southern Biotech) and images were acquired with a Zeiss AxioImager.Z1 microscope. For immunofluorescence experiments in cell lines, cells were cultured on coverslips until confluent and starved for 48 h. To quantify ciliary Gli2 and Gpr161 levels, cells were treated with 500 nM SAG or DMSO for 24 h after 24 h of serum starvation. Cells were fixed with 4% PFA for 10 min at room temperature and postfixed for 5 min with methanol at -20°C for γ-tubulin immunostaining. After blocking with 5% normal donkey serum, the cells were incubated with primary antibody solutions for 1 h at room temperature followed by treatment with secondary antibodies for 30 min along with DAPI. Primary antibodies used were against Gpr161 (1:200, custom-made) (Pal et al. 2016), acetylated α-tubulin (mAb 6-11B-1, Sigma; 1:2000), GFP (Abcam ab13970), Tulp3 (1:500, gift from Jonathan Eggenschwiler) (Norman et al. 2009), Gli2 (1:500, gift from Jonathan Eggenschwiler) (Cho et al. 2008) , γ-tubulin (GTU-88, Sigma; 1:500). Coverslips were mounted with Fluoromount-G and images were acquired with a Zeiss AxioImager.Z1 microscope using a 40 × oil immersion objective lens.

Reverse transcription, quantitative PCR and Gli1/2/3 immunoblotting.
RNA was extracted using the GenElute mammalian total RNA purification kit (RTN350; Sigma). Genomic DNA was eliminated by DNase I (D5307; Sigma). qRT-PCR was performed with SYBR Green Quantitative RT-qPCR Kit (QR0100; Sigma) or Kicqstart One-Step Probe RT-qPCR ReadyMix (KCQS07; Sigma). *Gli1* (Wen et al. 2010) and *Ptch2* (Somatilaka et al. 2020) TaqMan probes for qRT-PCR were published before. Inventoried probes for *Gpr161*, and *Gapdh* were from Applied Biosystems. Reactions were run in CFX96 Real time System (Bio Rad). Embryos or limb buds were processed for Gli1/2/3 immunoblotting as described previously (Wen et al., 2010), using Gli3 (AF3690, R&D, 1ug/ml), Gli2 (AF3635, R&D, 1ug/ml), Gli1 (L42B10, Cell Signaling; 1:1000) and α-tubulin (clone DM1A, T6199, Sigma; 1:5000) antibodies.

In situ hybridization (ISH)
Antisense riboprobes were made using the following templates: *Ptch1, Gli1, Shh,* (gifts from Andrew McMahon lab and Deanna Grant, Andrew Peterson lab), *Sox9*, *Col2a1* (from Steven Vokes lab, UT Austin), *Hoxd13* (from Xin Sun lab, University of Wisconsin, Madison). Whole mount in situ hybridization using digoxigenin-labeled probes was performed on embryos using standard protocols. Images were acquired using a Leica stereomicroscope (M165 C) with digital camera (DFC500) or Zeiss stereomicroscope (Discovery.V12) and AxioCam MRc.

QUANTIFICATION AND STATISTICAL ANALYSIS
Cilia positive for acetylated α-tubulin and GPR161/TULP3 were counted and expressed as % of GPR161/TULP3 positive cilia. To quantify ciliary pools of GPR161 and TULP3, fluorescence levels were measured using the “Measure” tool of Fiji software. Fluorescence levels of neighboring background areas were subtracted from that of the selected ciliary areas and expressed as corrected fluorescence. Statistical analyses were performed using Student’s *t*-test for comparing two groups using GraphPad Prism.

Acknowledgements

This paper is dedicated to the memory of Kathryn Anderson, who has been a constant source of encouragement and inspiration in our studies on ciliary signaling. This project was funded by Alex's Lemonade Foundation (A-grant to S.M.) (grant #I-1906 to SM), and National Institutes of Health (1R01GM113023 to SM). We thank UT Southwestern's transgenic and mouse animal care facility. We acknowledge gifts of reagents from Rajat Rohatgi, Jonathan Eggenschwiler, Andrew McMahon, Deanna Grant, Andrew Peterson, Steven Vokes and Xin Sun. We thank Mukhopadhyay lab members for comments on the manuscript. Monoclonal antibodies developed by O.D. Madsen (Nkx6.1) and A. Kawakami (Pax7) were obtained from the Developmental Studies Hybridoma Bank developed under the auspices of the NICHD and maintained by the Department of Biological Sciences, the University of Iowa, Iowa City IA 52242, USA.

Author contributions

S. H. and S. M conceived the project, designed experiments, analyzed most of the data, and wrote the paper with inputs from all authors. S. H. performed most of the experiments. B. N. S. and K. W. performed cryosectioning and immunofluorescence experiments.

Competing Financial Interest Statement

The authors have no competing financial interests to declare.

References

Anvarian Z, Mykytyn K, Mukhopadhyay S, Pedersen LB, Christensen ST. 2019. Cellular signalling by primary cilia in development, organ function and disease. *Nat Rev Nephrol* **15**: 199-219.

Bachmann VA, Mayrhofer JE, Ilouz R, Tschaikner P, Raffeiner P, Rock R, Courcelles M, Apelt F, Lu TW, Baillie GS et al. 2016. Gpr161 anchoring of PKA consolidates GPCR and cAMP signaling. *Proc Natl Acad Sci U S A* **113**: 7786-7791.

Badgandi HB, Hwang SH, Shimada IS, Loriot E, Mukhopadhyay S. 2017. Tubby family proteins are adapters for ciliary trafficking of integral membrane proteins. *J Cell Biol* **216**: 743-760.

Bai CB, Joyner AL. 2001. Gli1 can rescue the in vivo function of Gli2. *Development* **128**: 5161-5172.

Bai CB, Stephen D, Joyner AL. 2004. All mouse ventral spinal cord patterning by hedgehog is Gli dependent and involves an activator function of Gli3. *Dev Cell* **6**: 103-115.

Barzi M, Berenguer J, Menendez A, Alvarez-Rodriguez R, Pons S. 2010. Sonic-hedgehog-mediated proliferation requires the localization of PKA to the cilium base. *J Cell Sci* **123**: 62-69.

Begemann M, Waszak SM, Robinson GW, Jager N, Sharma T, Knopp C, Kraft F, Moser O, Mynarek M, Guerrini-Rousseau L et al. 2019. Germline GPR161 Mutations Predispose to Pediatric Medulloblastoma. *J Clin Oncol*: JCO1900577.

Briscoe J, Therond PP. 2013. The mechanisms of Hedgehog signalling and its roles in development and disease. *Nat Rev Mol Cell Biol* **14**: 416-429.

Brugmann SA, Allen NC, James AW, Mekonnen Z, Madan E, Helms JA. 2010. A primary cilia-dependent etiology for midline facial disorders. *Hum Mol Genet* **19**: 1577-1592.

Calebiro D, Nikolaev VO, Gagliani MC, de Filippis T, Dees C, Tacchetti C, Persani L, Lohse MJ. 2009. Persistent cAMP-signals triggered by internalized G-protein-coupled receptors. *PLoS Biol* **7**: e1000172.

Caspary T, Larkins CE, Anderson KV. 2007. The graded response to Sonic Hedgehog depends on cilia architecture. *Dev Cell* **12**: 767-778.

Chang CF, Chang YT, Millington G, Brugmann SA. 2016. Craniofacial Ciliopathies Reveal Specific Requirements for GLI Proteins during Development of the Facial Midline. *PLoS Genet* **12**: e1006351.

Charite J, McFadden DG, Olson EN. 2000. The bHLH transcription factor dHAND controls Sonic hedgehog expression and establishment of the zone of polarizing activity during limb development. *Development* **127**: 2461-2470.

Chavez M, Ena S, Van Sande J, de Kerchove d'Exaerde A, Schurmans S, Schiffmann SN. 2015. Modulation of Ciliary Phosphoinositide Content Regulates Trafficking and Sonic Hedgehog Signaling Output. *Dev Cell* **34**: 338-350.

Chen MH, Wilson CW, Li YJ, Law KK, Lu CS, Gacayan R, Zhang X, Hui CC, Chuang PT. 2009. Cilium-independent regulation of Gli protein function by Sufu in Hedgehog signaling is evolutionarily conserved. *Genes Dev* **23**: 1910-1928.

Cho A, Ko HW, Eggenschwiler JT. 2008. FKBP8 cell-autonomously controls neural tube patterning through a Gli2- and Kif3a-dependent mechanism. *Dev Biol* **321**: 27-39.

Constable S, Mukhopadhyay S. 2020. Ubiquitin Tunes Hedgehog in Matters of the Heart. *Dev Cell* **55**: 385-386.

Corbit KC, Aanstad P, Singla V, Norman AR, Stainier DY, Reiter JF. 2005. Vertebrate Smoothened functions at the primary cilium. *Nature* **437**: 1018-1021.

Crilly SE, Puthenveedu MA. 2020. Compartmentalized GPCR Signaling from Intracellular Membranes. *J Membr Biol*.

Degorce F, Card A, Soh S, Trinquet E, Knapik GP, Xie B. 2009. HTRF: A technology tailored for drug discovery - a review of theoretical aspects and recent applications. *Curr Chem Genomics* **3**: 22-32.

Dessaud E, McMahon AP, Briscoe J. 2008. Pattern formation in the vertebrate neural tube: a sonic hedgehog morphogen-regulated transcriptional network. *Development* **135**: 2489-2503.

Falkenstein KN, Vokes SA. 2014. Transcriptional regulation of graded Hedgehog signaling. *Semin Cell Dev Biol* **33**: 73-80.

Garcia-Gonzalo FR, Corbit KC, Sirerol-Piquer MS, Ramaswami G, Otto EA, Noriega TR, Seol AD, Robinson JF, Bennett CL, Josifova DJ et al. 2011. A transition zone complex regulates mammalian ciliogenesis and ciliary membrane composition. *Nat Genet* **43**: 776-784.

Gigante ED, Taylor MR, Ivanova AA, Kahn RA, Caspary T. 2020. ARL13B regulates Sonic hedgehog signaling from outside primary cilia. *Elife* **9**.

Goetz SC, Anderson KV. 2010. The primary cilium: a signalling centre during vertebrate development. *Nature reviews Genetics* **11**: 331-344.

Haycraft CJ, Banizs B, Aydin-Son Y, Zhang Q, Michaud EJ, Yoder BK. 2005. Gli2 and Gli3 localize to cilia and require the intraflagellar transport protein polaris for processing and function. *PLoS Genet* **1**: e53.

Hu D, Marcucio RS. 2009. Unique organization of the frontonasal ectodermal zone in birds and mammals. *Dev Biol* **325**: 200-210.

Hui CC, Angers S. 2011. Gli proteins in development and disease. *Annu Rev Cell Dev Biol* **27**: 513-537.

Humke EW, Dorn KV, Milenkovic L, Scott MP, Rohatgi R. 2010. The output of Hedgehog signaling is controlled by the dynamic association between Suppressor of Fused and the Gli proteins. *Genes Dev* **24**: 670-682.

Hwang SH, White KA, Somatilaka BN, Shelton JM, Richardson JA, Mukhopadhyay S. 2018. The G protein-coupled receptor Gpr161 regulates forelimb formation, limb patterning and skeletal morphogenesis in a primary cilium-dependent manner. *Development* **145**.

Irannejad R, Tomshine JC, Tomshine JR, Chevalier M, Mahoney JP, Steyaert J, Rasmussen SG, Sunahara RK, El-Samad H, Huang B et al. 2013. Conformational biosensors reveal GPCR signalling from endosomes. *Nature* **495**: 534-538.

Jia J, Kolterud A, Zeng H, Hoover A, Teglund S, Toftgard R, Liu A. 2009. Suppressor of Fused inhibits mammalian Hedgehog signaling in the absence of cilia. *Dev Biol* **330**: 452-460.

Kim J, Kato M, Beachy PA. 2009. Gli2 trafficking links Hedgehog-dependent activation of Smoothened in the primary cilium to transcriptional activation in the nucleus. *Proc Natl Acad Sci U S A* **106**: 21666-21671.

Kim SE, Lei Y, Hwang SH, Wlodarczyk BJ, Mukhopadhyay S, Shaw GM, Ross ME, Finnell RH. 2019. Dominant negative GPR161 rare variants are risk factors of human spina bifida. *Hum Mol Genet* **28**: 200-208.

Kopinke D, Norris AM, Mukhopadhyay S. 2020. Developmental and regenerative paradigms of cilia regulated hedgehog signaling. *Semin Cell Dev Biol*.

Kotowski SJ, Hopf FW, Seif T, Bonci A, von Zastrow M. 2011. Endocytosis promotes rapid dopaminergic signaling. *Neuron* **71**: 278-290.

Lee EC, Yu D, Martinez de Velasco J, Tessarollo L, Swing DA, Court DL, Jenkins NA, Copeland NG. 2001. A highly efficient Escherichia coli-based chromosome engineering system adapted for recombinogenic targeting and subcloning of BAC DNA. *Genomics* **73**: 56-65.

Leurs R, Smit MJ, Alewijnse AE, Timmerman H. 1998. Agonist-independent regulation of constitutively active G-protein-coupled receptors. *Trends Biochem Sci* **23**: 418-422.

Lewis AE, Vasudevan HN, O'Neill AK, Soriano P, Bush JO. 2013. The widely used Wnt1-Cre transgene causes developmental phenotypes by ectopic activation of Wnt signaling. *Dev Biol* **379**: 229-234.

Lex RK, Ji Z, Falkenstein KN, Zhou W, Henry JL, Ji H, Vokes SA. 2020. GLI transcriptional repression regulates tissue-specific enhancer activity in response to Hedgehog signaling. *Elife* **9**.

Li BI, Matteson PG, Ababon MF, Nato AQ, Jr., Lin Y, Nanda V, Matise TC, Millonig JH. 2015. The orphan GPCR, Gpr161, regulates the retinoic acid and canonical Wnt pathways during neurulation. *Dev Biol* **402**: 17-31.

Liu A, Wang B, Niswander LA. 2005. Mouse intraflagellar transport proteins regulate both the activator and repressor functions of Gli transcription factors. *Development* **132**: 3103-3111.

Liu J, Zeng H, Liu A. 2015. The loss of Hh responsiveness by a non-ciliary Gli2 variant. *Development* **142**: 1651-1660.

Logan M, Martin JF, Nagy A, Lobe C, Olson EN, Tabin CJ. 2002. Expression of Cre Recombinase in the developing mouse limb bud driven by a Prxl enhancer. *Genesis* **33**: 77-80.

Matteson PG, Desai J, Korstanje R, Lazar G, Borsuk TE, Rollins J, Kadambi S, Joseph J, Rahman T, Wink J et al. 2008. The orphan G protein-coupled receptor, Gpr161, encodes the vacuolated lens locus and controls neurulation and lens development. *Proc Natl Acad Sci U S A* **105**: 2088-2093.

Mick DU, Rodrigues RB, Leib RD, Adams CM, Chien AS, Gygi SP, Nachury MV. 2015. Proteomics of Primary Cilia by Proximity Labeling. *Dev Cell* **35**: 497-512.

Mo R, Freer AM, Zinyk DL, Crackower MA, Michaud J, Heng HH, Chik KW, Shi XM, Tsui LC, Cheng SH et al. 1997. Specific and redundant functions of Gli2 and Gli3 zinc finger genes in skeletal patterning and development. *Development* **124**: 113-123.

Mukhopadhyay S, Rohatgi R. 2014. G-protein-coupled receptors, Hedgehog signaling and primary cilia. *Semin Cell Dev Biol* **33**: 63-72.

Mukhopadhyay S, Wen X, Chih B, Nelson CD, Lane WS, Scales SJ, Jackson PK. 2010. TULP3 bridges the IFT-A complex and membrane phosphoinositides to promote trafficking of G protein-coupled receptors into primary cilia. *Genes Dev* **24**: 2180-2193.

Mukhopadhyay S, Wen X, Ratti N, Loktev A, Rangell L, Scales SJ, Jackson PK. 2013. The ciliary G-protein-coupled receptor Gpr161 negatively regulates the Sonic hedgehog pathway via cAMP signaling. *Cell* **152**: 210-223.

Murdoch JN, Copp AJ. 2010. The relationship between sonic Hedgehog signaling, cilia, and neural tube defects. *Birth Defects Res A Clin Mol Teratol* **88**: 633-652.

Nachury MV, Mick DU. 2019. Establishing and regulating the composition of cilia for signal transduction. *Nat Rev Mol Cell Biol* **20**: 389-405.

Niewiadomski P, Kong JH, Ahrends R, Ma Y, Humke EW, Khan S, Teruel MN, Novitch BG, Rohatgi R. 2014. Gli protein activity is controlled by multisite phosphorylation in vertebrate Hedgehog signaling. *Cell Rep* **6**: 168-181.

Niswander L. 2003. Pattern formation: old models out on a limb. *Nat Rev Genet* **4**: 133-143.

Norman RX, Ko HW, Huang V, Eun CM, Abler LL, Zhang Z, Sun X, Eggenschwiler JT. 2009. Tubby-like protein 3 (TULP3) regulates patterning in the mouse embryo through inhibition of Hedgehog signaling. *Hum Mol Genet* **18**: 1740-1754.

Oosterveen T, Kurdija S, Alekseenko Z, Uhde CW, Bergsland M, Sandberg M, Andersson E, Dias JM, Muhr J, Ericson J. 2012. Mechanistic differences in the transcriptional interpretation of local and long-range Shh morphogen signaling. *Dev Cell* **23**: 1006-1019.

Pal K, Hwang SH, Somatilaka B, Badgandi H, Jackson PK, DeFea K, Mukhopadhyay S. 2016. Smoothened determines beta-arrestin-mediated removal of the G protein-coupled receptor Gpr161 from the primary cilium. *The Journal of cell biology* **212**: 861-875.

Pan Y, Bai CB, Joyner AL, Wang B. 2006. Sonic hedgehog signaling regulates Gli2 transcriptional activity by suppressing its processing and degradation. *Mol Cell Biol* **26**: 3365-3377.

Persson M, Stamataki D, te Welscher P, Andersson E, Bose J, Ruther U, Ericson J, Briscoe J. 2002. Dorsal-ventral patterning of the spinal cord requires Gli3 transcriptional repressor activity. *Genes Dev* **16**: 2865-2878.

Pusapati GV, Kong JH, Patel BB, Gouti M, Sagner A, Sircar R, Luchetti G, Ingham PW, Briscoe J, Rohatgi R. 2018. G protein–coupled receptors control the sensitivity of cells to the morphogen Sonic Hedgehog. *Science Signaling* **11**: eaao5749.

Rohatgi R, Milenkovic L, Scott MP. 2007. Patched1 regulates hedgehog signaling at the primary cilium. *Science* **317**: 372-376.

Saade M, Gonzalez-Gobartt E, Escalona R, Usieto S, Marti E. 2017. Shh-mediated centrosomal recruitment of PKA promotes symmetric proliferative neuroepithelial cell division. *Nat Cell Biol* **19**: 493-503.

Sakai K, Miyazaki J. 1997. A transgenic mouse line that retains Cre recombinase activity in mature oocytes irrespective of the cre transgene transmission. *Biochem Biophys Res Commun* **237**: 318-324.

Schock EN, Brugmann SA. 2017. Discovery, Diagnosis, and Etiology of Craniofacial Ciliopathies. *Cold Spring Harb Perspect Biol* **9**.

Seifert R, Wenzel-Seifert K. 2002. Constitutive activity of G-protein-coupled receptors: cause of disease and common property of wild-type receptors. *Naunyn Schmiedebergs Arch Pharmacol* **366**: 381-416.

Shimada IS, Hwang SH, Somatilaka BN, Wang X, Skowron P, Kim J, Kim M, Shelton JM, Rajaram V, Xuan Z et al. 2018. Basal Suppression of the Sonic Hedgehog Pathway by the G-Protein-Coupled Receptor Gpr161 Restricts Medulloblastoma Pathogenesis. *Cell reports* **22**: 1169-1184.

Shimada IS, Somatilaka BN, Hwang SH, Anderson AG, Shelton JM, Rajaram V, Konopka G, Mukhopadhyay S. 2019. Derepression of sonic hedgehog signaling upon Gpr161 deletion unravels forebrain and ventricular abnormalities. *Dev Biol* **450**: 47-62.

Somatilaka BN, Hwang SH, Palicharla VR, White KA, Badgandi H, Shelton JM, Mukhopadhyay S. 2020. Ankmy2 Prevents Smoothened-Independent Hyperactivation of the Hedgehog Pathway via Cilia-Regulated Adenylyl Cyclase Signaling. *Dev Cell* **54**: 710-726 e718.

te Welscher P, Fernandez-Teran M, Ros MA, Zeller R. 2002. Mutual genetic antagonism involving GLI3 and dHAND prepatterns the vertebrate limb bud mesenchyme prior to SHH signaling. *Genes Dev* **16**: 421-426.

Tempe D, Casas M, Karaz S, Blanchet-Tournier MF, Concordet JP. 2006. Multisite protein kinase A and glycogen synthase kinase 3beta phosphorylation leads to Gli3 ubiquitination by SCFbetaTrCP. *Mol Cell Biol* **26**: 4316-4326.

Tschaikner P, Regele D, Salvenmoser W, Geley S, Stefan E, Aanstad P. 2019. Zebrafish GPR161 Contributes to Basal Hedgehog Repression in a Tissue-specific Manner. *bioRxiv*: 616482.

Tuson M, He M, Anderson KV. 2011. Protein kinase A acts at the basal body of the primary cilium to prevent Gli2 activation and ventralization of the mouse neural tube. *Development* **138**: 4921-4930.

Vilardaga JP, Jean-Alphonse FG, Gardella TJ. 2014. Endosomal generation of cAMP in GPCR signaling. *Nat Chem Biol* **10**: 700-706.

Wang B, Fallon JF, Beachy PA. 2000. Hedgehog-regulated processing of Gli3 produces an anterior/posterior repressor gradient in the developing vertebrate limb. *Cell* **100**: 423-434.

Wang C, Pan Y, Wang B. 2010. Suppressor of fused and Spop regulate the stability, processing and function of Gli2 and Gli3 full-length activators but not their repressors. *Development* **137**: 2001-2009.

Wen X, Lai CK, Evangelista M, Hongo JA, de Sauvage FJ, Scales SJ. 2010. Kinetics of hedgehog-dependent full-length Gli3 accumulation in primary cilia and subsequent degradation. *Mol Cell Biol* **30**: 1910-1922.

Ybot-Gonzalez P, Cogram P, Gerrelli D, Copp AJ. 2002. Sonic hedgehog and the molecular regulation of mouse neural tube closure. *Development* **129**: 2507-2517.

Ybot-Gonzalez P, Gaston-Massuet C, Girdler G, Klingensmith J, Arkell R, Greene ND, Copp AJ. 2007. Neural plate morphogenesis during mouse neurulation is regulated by antagonism of Bmp signalling. *Development* **134**: 3203-3211.

Yu W, Wang Y, McDonnell K, Stephen D, Bai CB. 2009. Patterning of ventral telencephalon requires positive function of Gli transcription factors. *Dev Biol* **334**: 264-275.

Zeidler MG, Van Keuren ML, Saunders TL. 2011. BAC Transgenes, DNA Purification, and Transgenic Mouse Production. in *Advanced Protocols for Animal Transgenesis: An ISTT Manual* (eds. S Pease, TL Saunders), pp. 159-179. Springer Berlin Heidelberg, Berlin, Heidelberg.

Zhao T, Gan Q, Stokes A, Lassiter RN, Wang Y, Chan J, Han JX, Pleasure DE, Epstein JA, Zhou CJ. 2014. beta-catenin regulates Pax3 and Cdx2 for caudal neural tube closure and elongation. *Development* **141**: 148-157.

Table 1. Results of breeding animals having *Gpr161 ko* and/or *mut1* alleles.

Breeding between *Gpr161 ko*/+ parents

	Litters	*wt/wt*	*ko/wt*	*ko/ko*
E9.5	13	22 (23%)	46 (49%)	26 (28%)
E10.25	5	9 (24%)	18 (47%)	11 (29%)
E10.5	6	14 (32%)	30 (68%)	0 (0%)

Breeding *Gpr161 ko*/+ with *Gpr161 mut1*/+ parents

	Litters	*wt/wt*	*ko/wt* or *mut1/wt*	*mut1/ko*
E9.5	11	25 (27%)	45 (50%)	21 (23%)
E10.25	4	8 (29%)	14 (50%)	6 (21%)
E10.5	2	3 (21%)	7 (50%)	4 (29%)
E11.5	2	3 (21%)	7 (50%)	4 (29%)
E12.5	5	14 (35%)	23 (58%)	3 (7%)*[1]
E13.5	2	3 (30%)	7 (70%)	0 (0%)*

Breeding between *Gpr161 mut1*/+ parents

	Litters	*wt/wt*	*mut1/wt*	*mut1/mut1*
E9.5	10	24 (28%)	37 (43%)	25 (29%)
E10.25	3	6 (25%)	13 (54%)	5 (21%)
E10.5	5	6 (16%)	20 (51%)	13 (33%)
E11.5	1	3 (50%)	1 (17%)	2 (33%)
E12.5	5	11 (28%)	20 (51%)	8 (21%)
E13.5	7	11 (24%)	23 (50%)	12 (26%)
E14.5	1	2 (40%)	2 (40%)	1 (20%)*[2]
E15.5	1	1 (33%)	2 (66%)	0 (0%)*[3]

* Dead or resorbed embryos were not counted.

[1] 3 dead *mut1/ko* embryos were not counted

[2] 1 dead *mut1/mut1* embryo was not counted

[3] 2 dead *mut1/mut1* embryos were not counted

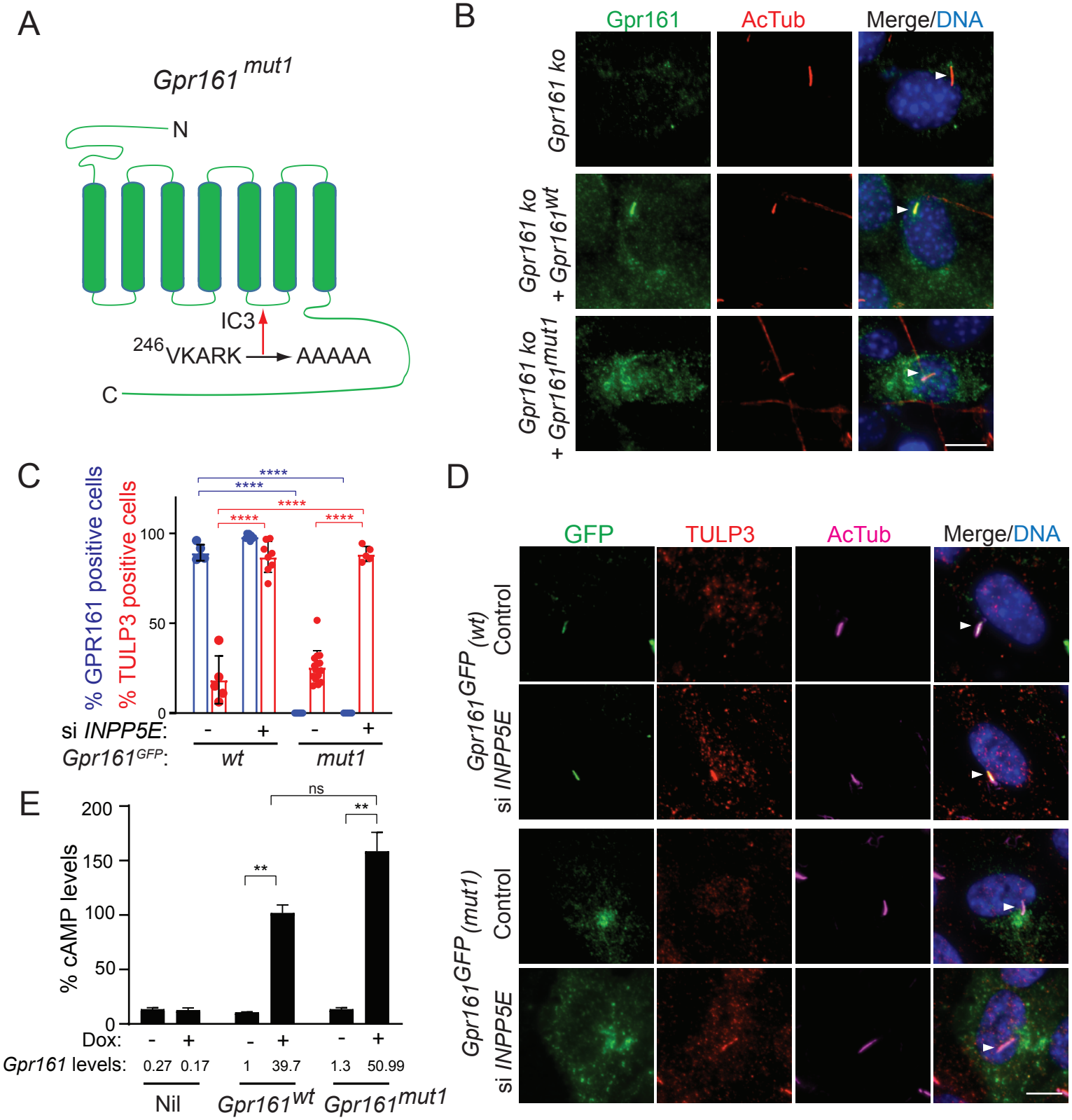

Figure 1. A ciliary localization defective *Gpr161* mutant is competent for cAMP signaling.

(A) Cartoon representing the VKARK>AAAAA mut1 mutation in the third intracellular loop of mouse Gpr161.

(B) Confluent NIH 3T3 Flp-In CRISPR-based *Gpr161* knockout (ko) cells stably expressing untagged wildtype (wt) or Gpr161^{mut1} were starved for 24h, fixed, and immunostained with anti-Gpr161 (green), anti-acetylated tubulin (AcTub; red) antibodies and counterstained for DNA (blue). Arrowheads indicate cilia.

(C) – (D) RPE hTERT cells stably expressing C-terminal LAP-tagged *Gpr161*^{wt} or *Gpr161*^{mut1} constructs were sequentially transfected with control or *INPP5E* siRNA (100 nM) twice and cultured for a total of 72 h. The cells were serum starved for the last 24 h before fixation and immunostained with anti-GFP (green), anti-TULP3 (red), anti-acetylated tubulin (AcTub; magenta) antibodies and counterstained for DNA (blue). GPR161 and TULP3 positive cells were quantified. Arrowheads in (D) indicate cilia. Total 6-12 different images quantified from 2 experiments, and total 600-2000 cells counted/condition. Data shown as mean ± SD. ****, $p<0.0001$. Other pairwise comparisons are not significantly different.

(E) Doxycycline-inducible NIH 3T3 Tet-on 3G cells expressing untagged *Gpr161*^{wt} or *Gpr161*^{mut1} were induced for 24h with 2μg/ml doxycycline. The cells were subjected to TR-FRET cell-based assays for assaying cAMP. cAMP levels were calculated as % values of uninduced Gpr161 expressing cells. Data from triplicate wells (mean ± SD) and is representative of 3 independent experiments. Mean *Gpr161* transcript levels are shown below. **, $p<0.01$. ns, not significant.

Scale: (B) and (D), 10 μm.

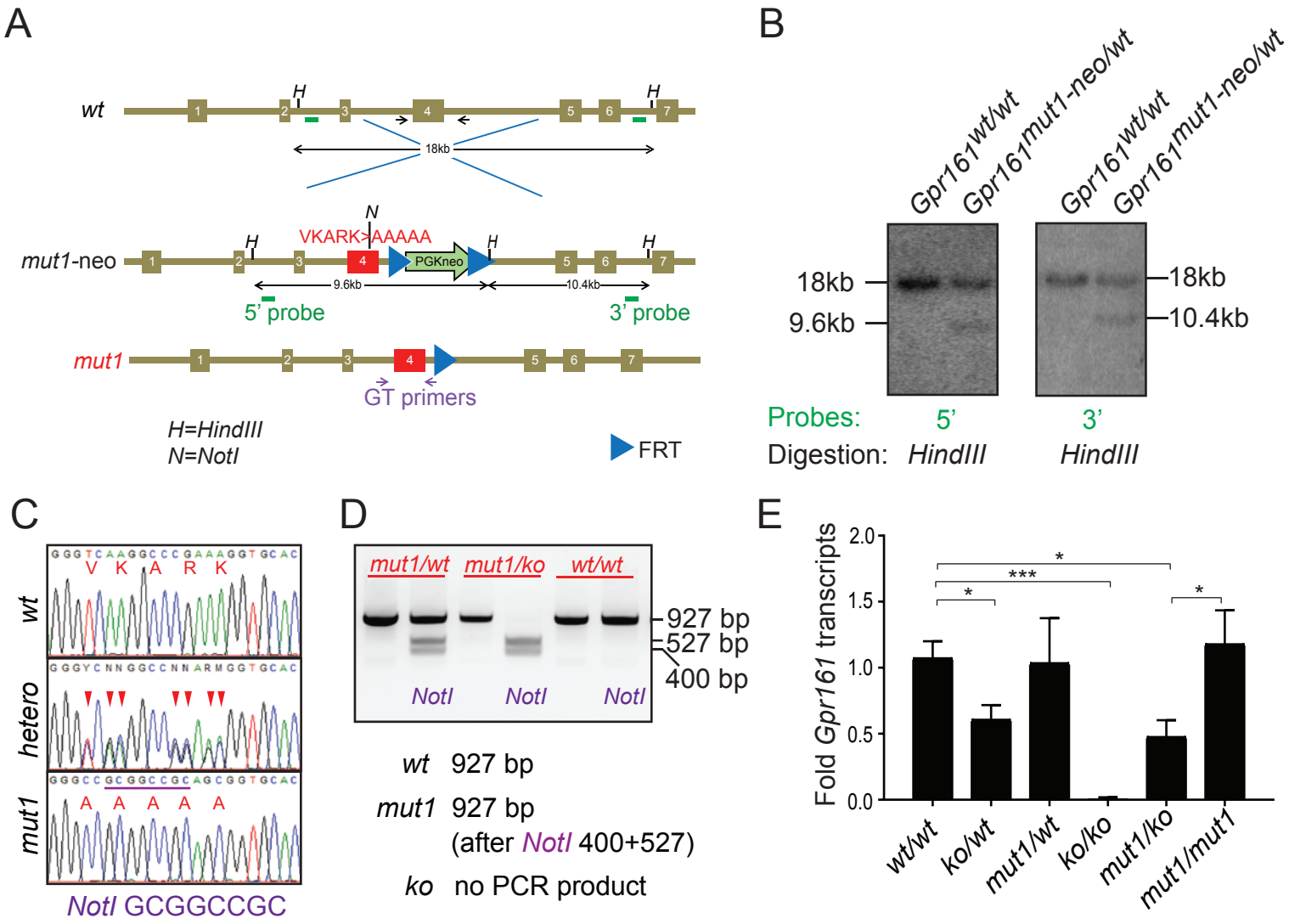

Figure 2. Generating ciliary localization defective endogenous knock-in *Gpr161^{mut1}* mouse model.

(A) The gene targeting strategy used to engineer the *Gpr161^{mut1}* allele. Exons are numbered based on NM_001081126.2. PGKneo and FRT cassettes and genotyping (GT) primer sequences are indicated. The *mut1* sequence is located on Exon 4.

(B) Southern blot analysis of representative ES cell clones using the 5' and 3' probes in A.

(C) Sanger sequencing of *Gpr161^{wt}* and *Gpr161^{mut1}* alleles in adult mouse-tail DNA. Double peaks in *Gpr161$^{wt/mut1}$* heterozygote indicated by arrowheads. The engineered NotI restriction site (GCGGCCGC) is indicated by a purple bar.

(D) Genotyping for wild type, *Gpr161^{mut1}* and knockout (ko) alleles by PCR using designated primers shown in A and digesting with NotI.

(E) qRT-PCR of *Gpr161* transcripts normalized to *Hprt* in whole embryo extracts at E9.5 indicate diminished mRNA expression in the *Gpr161* knockout (*ko/ko*) embryos compared to wild type (*wt/wt*), but unchanged in *mut1/mut1* embryos. Data shown as mean ± SD. n=3 (*wt/wt*), 5 (*ko/wt*), 4 (*mut1/wt*), 3 (*ko/ko*), 3 (*ko/mut1*), 2 (*mut1/mut1*) embryos. *, p<0.05; ***, p<0.001. Other pairwise comparisons are not significantly different.

Figure 2- figure supplement 1.

(A) Genomic DNA sequence of *Gpr161mut1* allele, after deletion of the FRT-PGKneo-FRT cassette by crossing with Flp-O mice. Exon 4 in tan color.

(B) Scheme for generating *mut1* allele. Details in Methods.

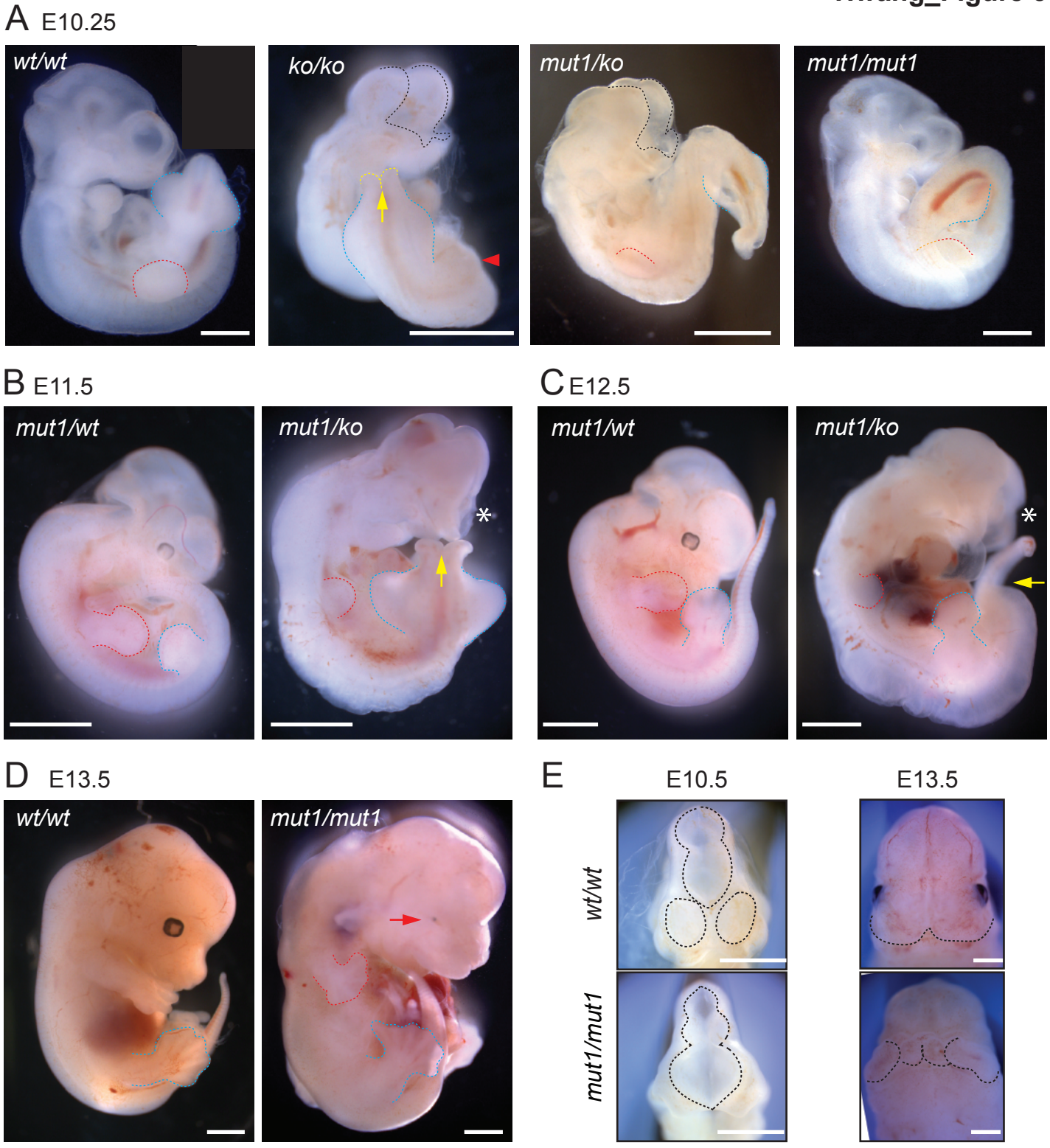

Figure 3. *Gpr161*^{mut1} allele is hypomorphic to knockout.

(A) – (F) Bright-field images of wild type (*wt/wt*), *Gpr161* knockout (*ko/ko*), *mut1/ko* heterozygote, and *mut1* homozygote (*mut1/mut1*) at indicated time points. Red arrowhead indicates no limb bud in knockout embryo. *En face* view of E10.5 and E13.5 embryos in (E). Black dotted line or asterisk, rostral malformation; yellow arrow and dotted line, spina bifida; red dotted line, forelimb; blue dotted line, hindlimb.

Scale: (A), 1 mm; (B-D), 2 mm; (D); (E), 1 mm.

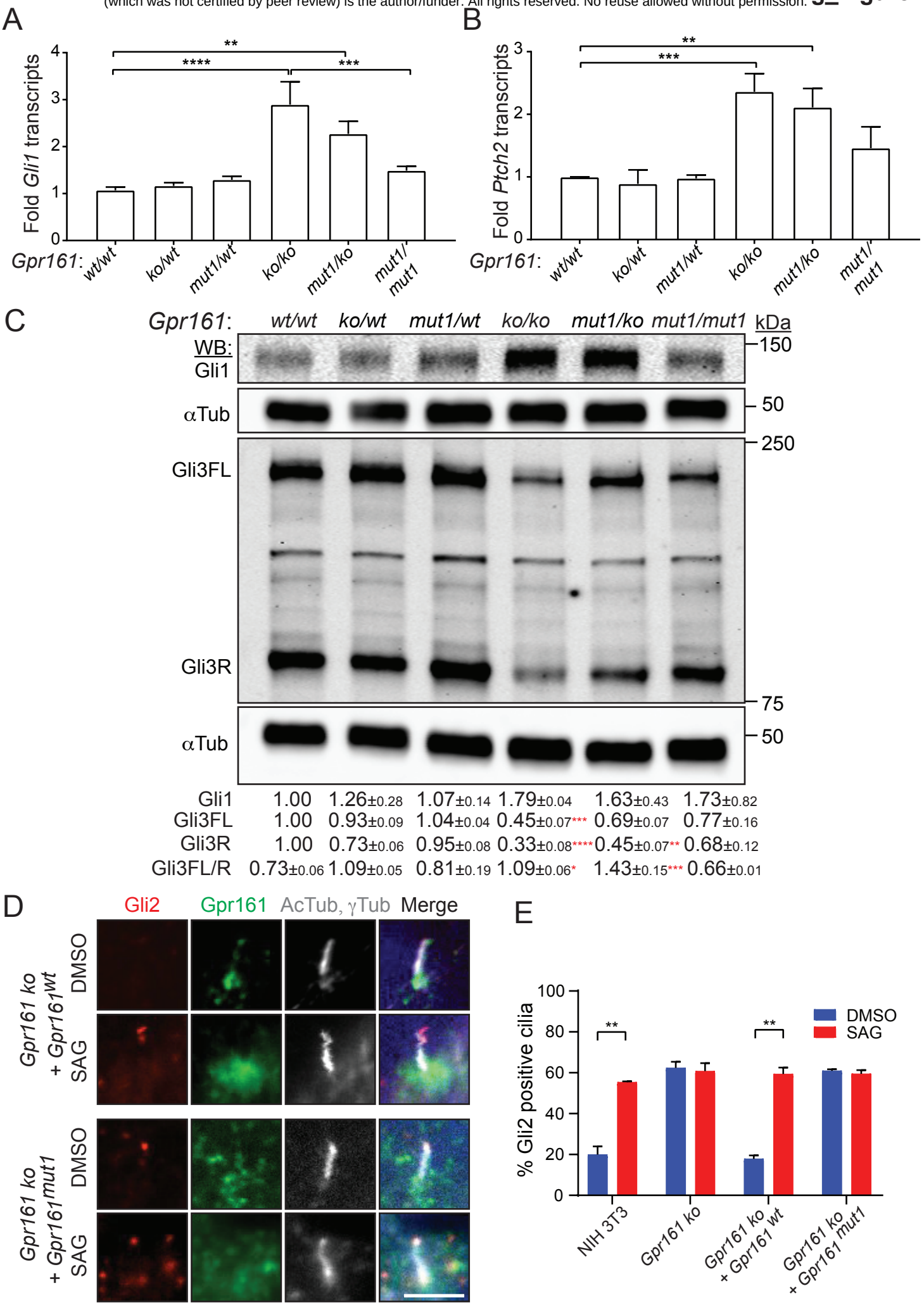

Figure 4. *Gpr161*$^{mut1/ko}$ embryos have reduced Hh pathway hyperactivation compared to knockouts.

(A) – (B) *Gli1* (A) and *Ptch2* (B) transcript levels in whole-embryo extracts at E9.5 qRT-PCR, normalized to *Gapdh*, n = 3-4 embryos each, data shown as mean ± SEM. **, p<0.01, ***, p<0.001, ****, p<0.0001. Only significant differences are marked.

(C) Immunoblotting for Gli1, Gli3 and α-tubulin in whole-embryo lysates at E9.5. n=2 or 3 independent experiments for Gli1 or Gli3 immunoblotting, respectively. Data shown as mean ± SD normalized to α-tubulin. *, p<0.05; **, p<0.01; ***, p<0.001; ****, p<0.0001.

(D) NIH 3T3 Flp-In CRISPR based *Gpr161* ko cells stably expressing untagged wildtype (*wt*) or *Gpr161*^{mut1} were starved for 24 h upon confluence and were treated for further 24 h ± SAG (500 nM). After fixation, cells were immunostained with anti-Gli2 (red), anti-Gpr161 (green), anti-acetylated and γ-tubulin (AcTub; γTub grey) antibodies.

(E) Quantification of Gli2 positive cilia from (D). n=100 cells counted/condition from two coverslips each. Data shown as mean ± SD. **, p<0.01.

Scale: (E), 5 μm.

Figure 4-figure supplement 1. Immunoblotting for Gli2 and α-tubulin in E9.5 whole-embryo lysates. n = 2. Data shown as mean ± SD.

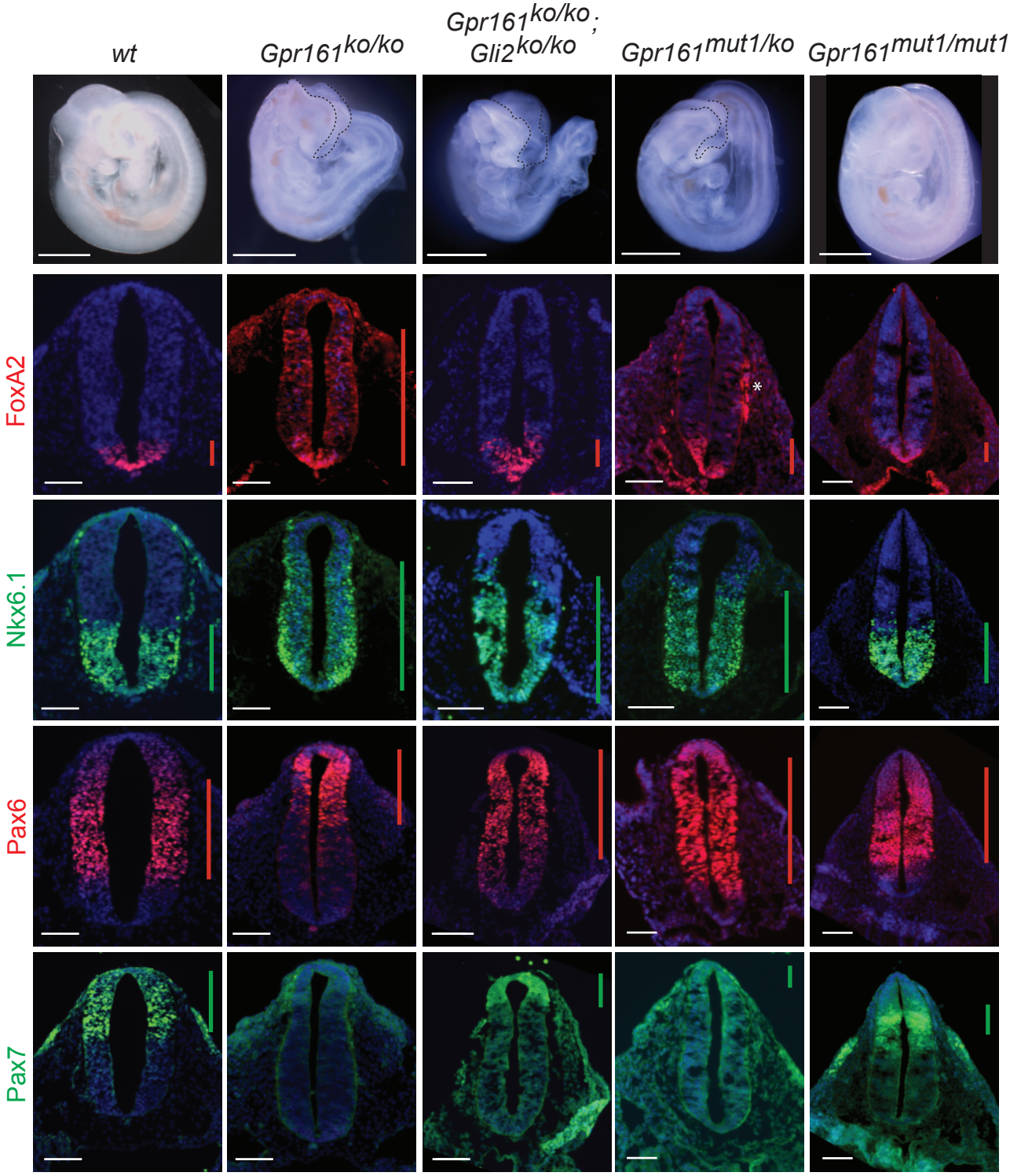

Figure 5. *Gpr161*$^{mut1/ko}$ embryos exhibit less ventralized neural tube compared to *Gpr161* knockouts.

Topmost panels show bright-field images of wildtype (*wt*), *Gpr161 ko, Gpr161 mut1/ko, Gpr161 mut1/mut1, Gpr161; Gli2* double *ko*, and *Gli2 ko* whole-mount embryos at E9.5. Bottom panels show thoracic neural tube horizontal sections immunostained using designated markers. All images are counterstained with Hoechst. Black dotted line mark rostral malformations. Vertical bars show the extent of dorsoventral expression of markers. Asterix, nonspecific background staining outside neural tube. n=2 to 4 embryos each genotype and immunostaining.
Scale: 50 μm.

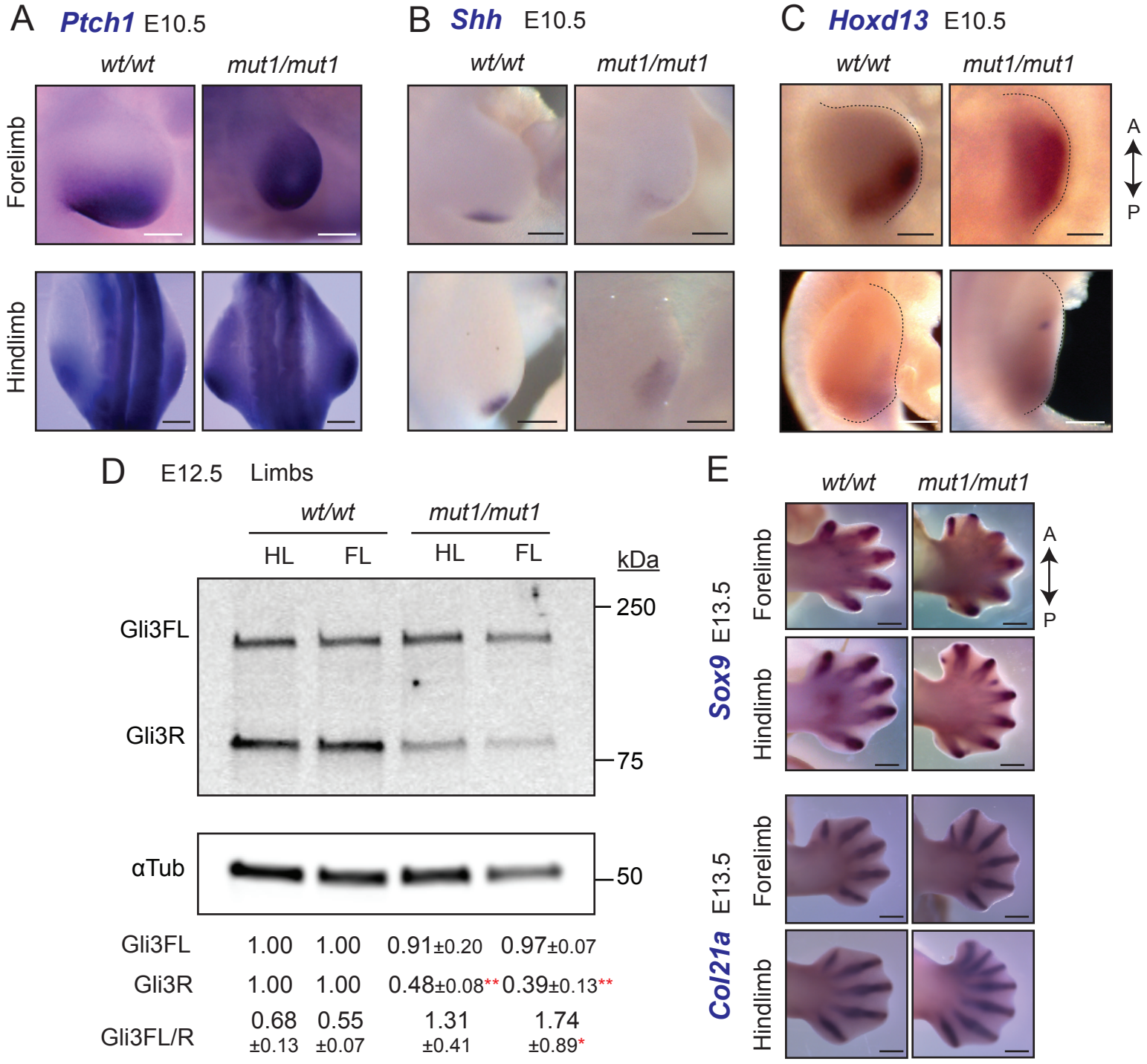

Figure 6. *Gpr161*$^{mut1/mut1}$ embryos exhibit high Hh signaling and polydactyly in limb buds.

(A) – (C) RNA *in situ* hybridization for E10.5 *Ptch1* (A), *Shh* (B) *Hoxd13* (C) limb buds. Control (*Gpr161*$^{mut1/wt}$) in (A-B). *Ptch1* and *Hoxd13* were expanded anteriorly in *Gpr161*$^{mut1/mut1}$ limb buds. Shh was diffusely expressed posteriorly but was not ectopically expressed anteriorly in *Gpr161*$^{mut1/mut1}$ limb buds. n=2-5 each.

(D) Immunoblotting of forelimb (FL) and hindlimb (HL) buds for Gli3 and α-tubulin shows decreased Gli3R levels at E12.5 wildtype (wt) versus *Gpr161*$^{mut1/mut1}$. Quantification shown is normalized to α-tubulin. n = 3 experiments. *, p<0.05; **, p<0.01.

(E) RNA *in situ* hybridization for *Sox9* and *Col2a1* in E13.5 wildtype and *Gpr161*$^{mut1/mut1}$ limb buds. *Gpr161*$^{mut1/mut1}$ limb buds show polydactyly. n=4 each.

Scale: (A-C), 50 μm; (E), 500 μm.

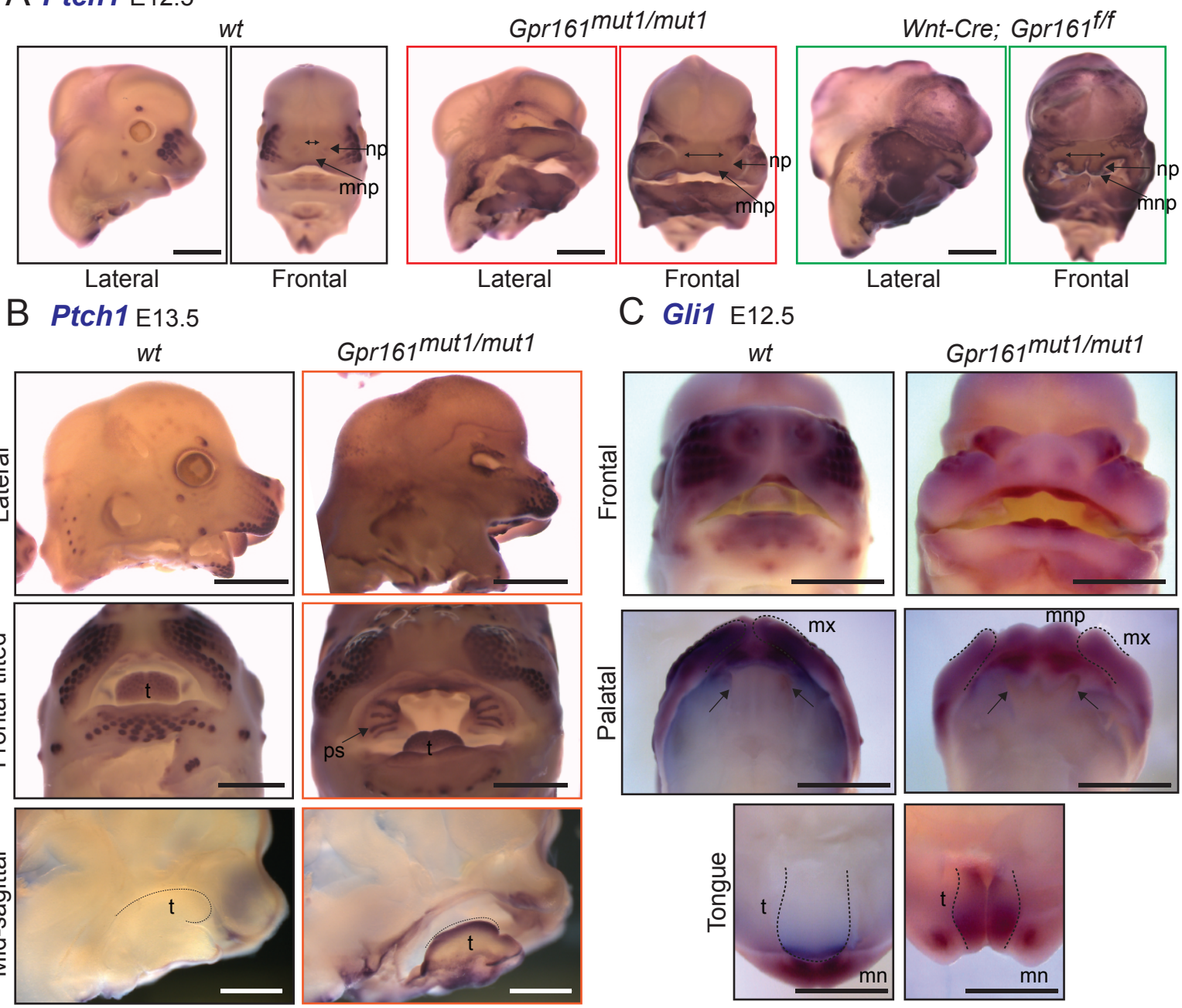

Figure 7. *Gpr161$^{mut1/mut1}$* embryos show high Hh signaling and mid face widening.

(A) RNA *in situ* hybridization for *Ptch1* in wildtype (*wt*), *Gpr161$^{mut1/mut1}$*, and *Wnt1-Cre*; *Gpr161$^{f/f}$* E12.5 head. Distances between nasal pits are shown as bidirectional arrows. Lateral and frontal views are shown. n=3-4 each

(B) RNA *in situ* hybridization for *Ptch1* in E13.5 wildtype (*wt*), *Gpr161$^{mut1/mut1}$* head. Top panels, lateral view; middle panels, frontal tilted view shows palate and tongue; bottom panels, sagittal section showing tongue. Black dotted lines in the bottom panels indicate tongue. Bidirectional arrows show increased distance between nasal pits. Arrow points to prominent palatal shelf in *Gpr161$^{mut1/mut1}$*. n=3 each

(C) RNA *in situ* hybridization for *Gli1* in E12.5 wildtype (*wt*), *Gpr161$^{mut1/mut1}$* head. Top panels, frontal view. Middle panels show palates imaged from below (palatal view) and bottom panels show lower jaw viewed from above (tongue view) after separating the jaws. Arrows in upper panel show secondary palatal shelves. Black dotted lines in the bottom panels indicate tongue. Note increased gap between maxillary processes by ingression of median nasal processes. n=3 each

(D) – (E) Quantification of distance between nasal pits as shown in (A). The colors are matched with each strain in A and B. Error bars represent SEM. ***, P<0.001; ****, P<0.0001, unpaired t-test. n=3-4 each.

(F) RNA *in situ* hybridization for *Ptch1* in E12.5 control (*Gli2$^{-/+}$*), *Gpr161; Gli2* double ko and *Gli2* ko head. Note persistent exencephaly in *Gpr161; Gli2* double ko and midfacial widening. Displaced lower jaw is an artifact (*). n=1-2 each

Scale: (A) and (F), 1 mm; (B) and (C) 2 mm.

Abbreviations: ex, exencephaly; mnp, medial nasal process; mx, maxillary process; mn, mandibular process; np, nasal pit; ps, palatal shelf; t, tongue

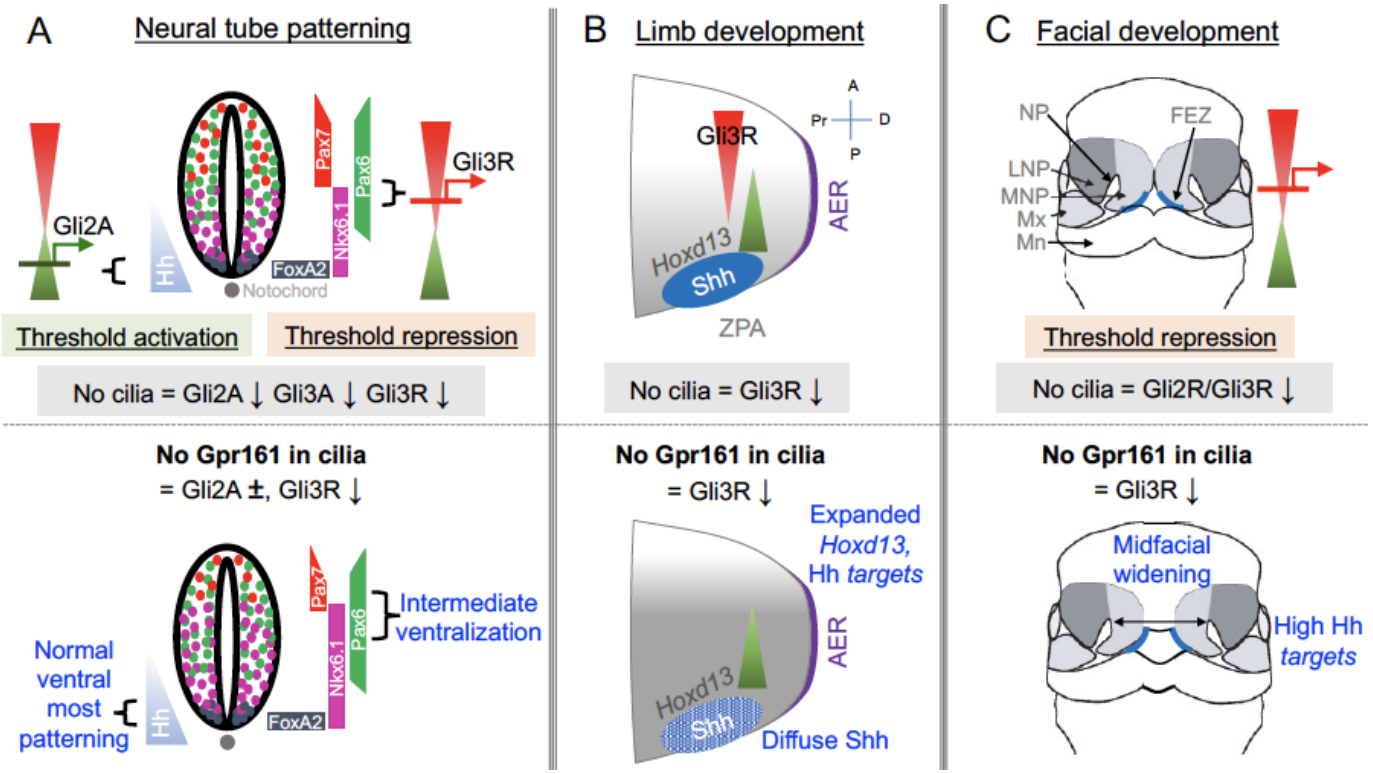

Figure 8. Gpr161 ciliary pools determine Hh pathway repression-regulated morpho-phenotypic spectrum.

(A) Neural tube development. Hh is expressed from the notochord (blue). Gli2A-mediated threshold activation mediates floorplate and ventral most progenitor patterning. Gli3R regulates intermediate level patterning. Lack of cilia prevents patterning of all ventral progenitors. Complete lack of Gpr161 in ko causes ventralization of all ventral progenitors from excessive Gli2A generation and loss of Gli3R. Lack of Gpr161 ciliary pools in *Gpr161*$^{mut1/ko}$ reduces Gli3R formation sufficiently to cause intermediate level expansion of Nkx6.1 but does not generate excessive GliA to cause ventralization of floor plate markers. Caudal spina bifida and exencephaly persists in *Gpr161*$^{mut1/ko}$ embryos similar to *Gpr161* ko.

(B) Limb development. Before Shh expression, Gli3R gradient is set up by posterior dHand gradient that is established in posterior mesenchyme. Shh expression from ZPA starting from E9.75 establishes posterior gradient of pathway targets such as *Ptch1/Gli1*. Anterior Gli3R gradient also regulates expression of genes in posterior mesenchyme such as *Hoxd13*. Lack of cilia causes preaxial polydactyly from increased *5'Hoxd* gene expression arising from lack of Gli3R. *Gpr161* ko prevents forelimb formation. Conditional deletion of *Gpr161* in limb mesenchyme causes increased Hh pathway targets, expanded *Hoxd13* and lack of Gli3R in limb buds contributing to polydactyly. Lack of Gpr161 ciliary pools in *Gpr161*$^{mut1/mut1}$ shows increased Hh pathway targets, expanded *Hoxd13* and lack of Gli3R in limb buds contributing to polydactyly. The Shh expression in the posterior limb bud is diffuse, likely from lack of counter-antagonism between Gli3R and dHand. Abbreviations: AER, anterior ectodermal ridge; ZPA, zone of polarizing activity; A, anterior; P, posterior, Pr, proximal; D, distal.

(C) Facial development. Shh is expressed from the frontonasal ectodermal zone in the medial nasal processes. Threshold repression by both Gli2R and Gli3R prevents midfacial widening. Lack of cilia, or lack of both Gli2/3 causes midfacial widening, which is prevented by forced Gli3R expression. Lack of Gpr161 ciliary pools in *Gpr161*$^{mut1/mut1}$ phenocopies *Gpr161* deletion in craniofacial mesenchyme in showing midfacial widening and increased levels of Shh pathway targets. Gli2 loss is unable to rescue midfacial widening and increased Shh pathway targets in *Gpr161* ko background, suggesting lack of GliR contributing to these phenotypes. Abbreviations: FEZ, frontonasal ectodermal zone; LNP, lateral nasal process; MNP, medial nasal process, Mx, maxillary process.

Hwang_Figure 2- Supplement 1

A *Gpr161* Exon 4 mutation

V K A R K → A A A A A

GTCAAGGCCCGAAAG → GcCgcGGCCgcAgcG

NotI

ctaaatgtttttaaaaggcaatacagaaagcaacagcaaagcaaatagaaagcagattaggataattcctctctcccctc
cctgtcttcttttctagCTACTACGCCGTCCTGTATCCAATGGTGTACCCCATGAAGATCACAG
GGAACCGAGCTGTGATGGCTCTCGTCTACATCTGGCTCCACTCTCTCATTGGCTGT
CTGCCGCCCCTATTTGGTTGGTCATCGGTGGAGTTTGATGAGTTCAAGTGGATGTG
TGTGGCCGCGTGGCACCAGGAACCCGGCTACACCATTTTCTGGCAGATCTGGTGT
GCCCTGTTCCCCTTTCTCATCATGCTAGTGTGCTACGGTTTCATCTTCCGGGTGGC
CAGG**GcCgcGGCCgcAgcG**GTGCACTGTGGCACGGTGGTCACTGTGGAGGAGGA
CTCTCAGAGGAGCGGGAGGAAGAATTCTAGTACCTCCACTTCCTCCTCCGGCAGT
AGGAGGAATGCCCTTCAAGGAGTGGTCTATTCAGCTAACCAGTGCAAAGCCCTCAT
CACCATCCTGGTGGTCATTGGCGCCTTCATGGTCACCTGGGGCCCCTACATGGTT
GTCATTACCTCAGAGGCACTCTGGGGGAAGAACTGTGTCTCCCCAACCCTGGAGA
CTTGGGCCACATGGCTGTCCTTTACCAGTGCCATCTGCCACCCTCTGATCTACGGA
CTCTGGAACAAGACTGTGCGCAAGGAGCTCCTGGGCATGTGCTTTGGGGACCGT
TATTACCGGGAATCCTTTGTGCAGCGACAGAGGACCTCCAGGCTCTTCAGCATTTC
CAACAGGATCACAGgtaactaggaaaaagaccctcacacctcaggcagatgtcacccggggtccttcccagtg
gctaagggcagtgtcagggtggctgtggtctcaaggctgaagcggccgcGAAGTTCCTATTCTCTAGAAA
GTATAGGAACTTCattctaccgggtaggggaggcgcttttcccaaggcagtctggagcatgcg

B *Gpr161*^{mut1} allele in BAC

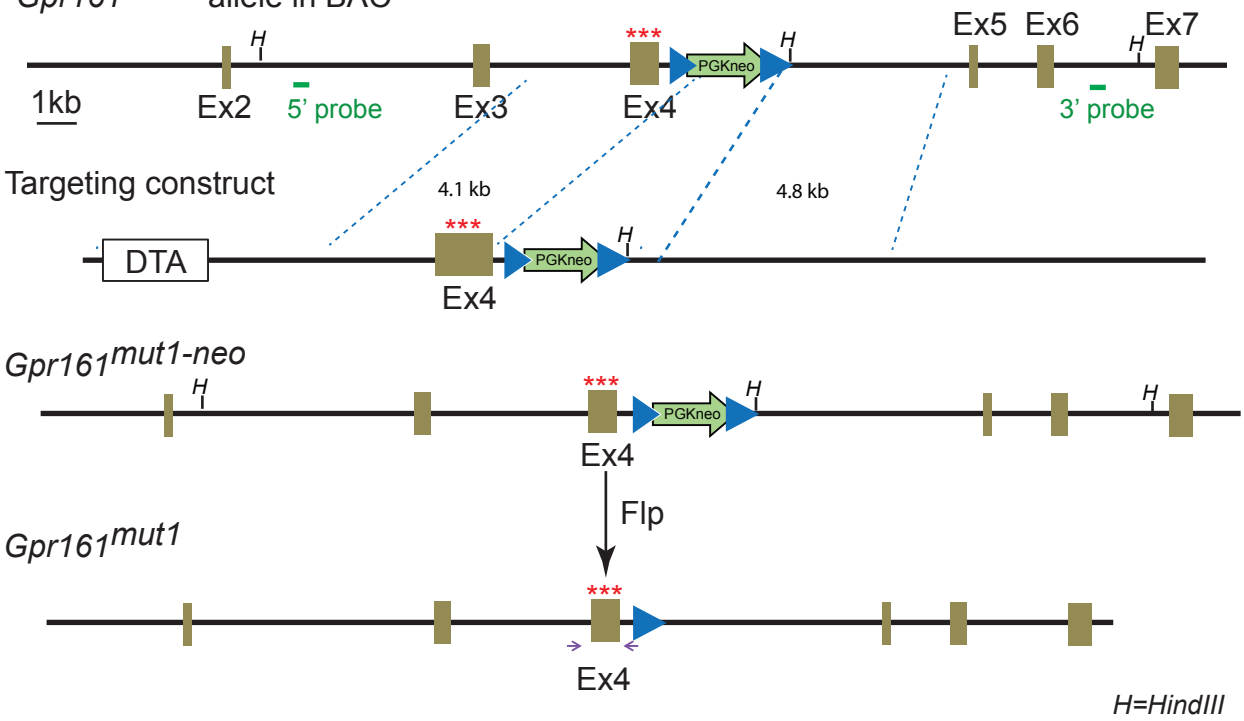

Figure 2- figure supplement 1.

(A) Genomic DNA sequence of *Gpr161mut1* allele, after deletion of the FRT-PGKneo-FRT cassette by crossing with Flp-O mice. Exon 4 in tan color.

(B) Scheme for generating *mut1* allele. Details in Methods.

.

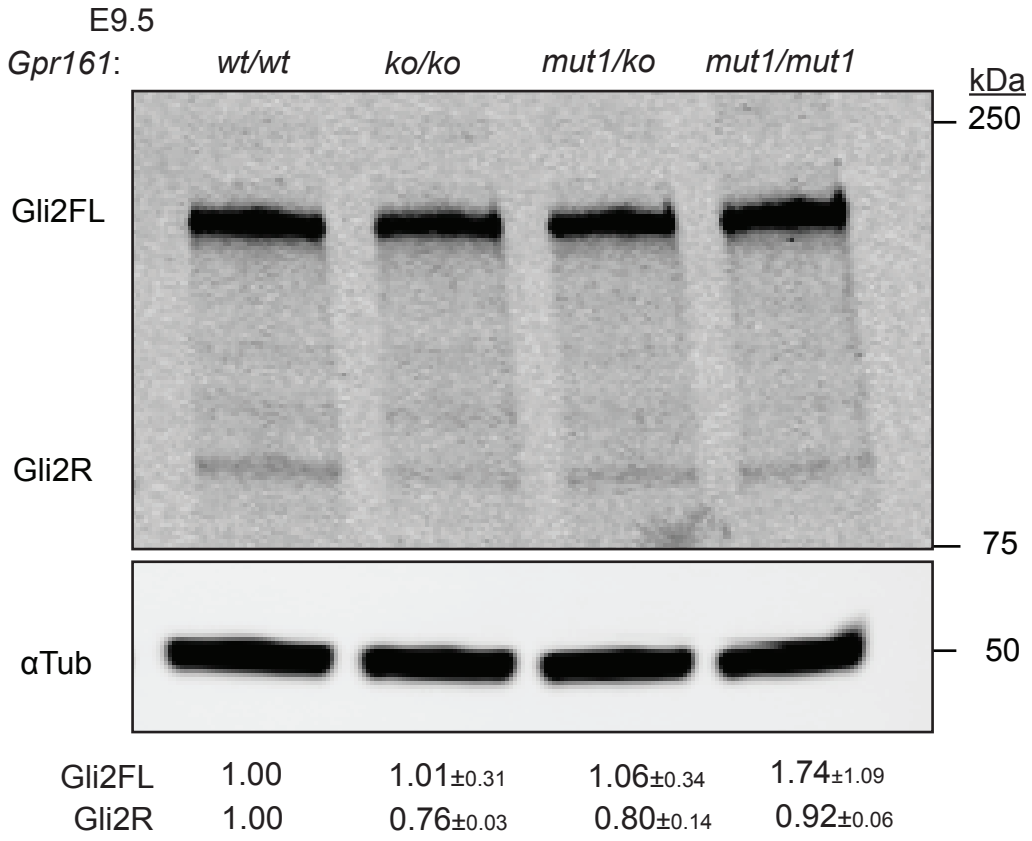

Figure 4-figure supplement 1. Immunoblotting for Gli2 and α-tubulin in E9.5 whole-embryo lysates. n = 2. Data shown as mean ± SD.